Journal Pre-proof

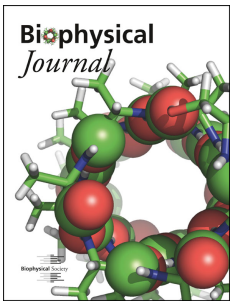

A Tridomain Model for Potassium Clearance in Optic Nerve of Necturus

Yi Zhu, Shixin Xu, Robert.S. Eisenberg, Huaxiong Huang

PII: S0006-3495(21)00507-5

DOI: https://doi.org/10.1016/j.bpj.2021.06.020

Reference: BPJ 11179

To appear in: *Biophysical Journal*

Received Date: 11 December 2020

Accepted Date: 14 June 2021

Please cite this article as: Zhu Y, Xu S, Eisenberg RS, Huang H, A Tridomain Model for Potassium Clearance in Optic Nerve of Necturus, *Biophysical Journal* (2021), doi: https://doi.org/10.1016/j.bpj.2021.06.020.

This is a PDF file of an article that has undergone enhancements after acceptance, such as the addition of a cover page and metadata, and formatting for readability, but it is not yet the definitive version of record. This version will undergo additional copyediting, typesetting and review before it is published in its final form, but we are providing this version to give early visibility of the article. Please note that, during the production process, errors may be discovered which could affect the content, and all legal disclaimers that apply to the journal pertain.

© 2021 Biophysical Society.

Journal Pre-proof

A Tridomain Model for Potassium Clearance in Optic Nerve of Necturus

Yi Zhu[1], Shixin Xu[2,*], Robert.S. Eisenberg[3,4], and Huaxiong Huang[5,6,1,*]

[1]Department of Mathematics and Statistics, York University, Toronto, ON, M3J 1P3, Canada
[2]Zu Chongzhi Center for Mathematics and Computational Sciences, Division of Natural and Applied Sciences, Duke Kunshan University, 8 Duke Ave., Kunshan, Jiangsu,215316, China
[3]Department of Applied Mathematics, Illinois Institute of Technology, Chicago IL 60616 USA
[4]Department of Physiology & Biophysics, Rush University Chicago IL 60612, USA
[5]Research Centre for Mathematics, Advanced Institute of Natural Sciences, Beijing Normal University (Zhuhai), 519087, China
[6]Division of Science and Technology, BNU- HKBU United International College, Zhuhai, 519087, China

[*]Correspondence: shixin.xu@dukekunshan.edu.cn, hhuang@uic.edu.cn

Abstract Complex fluids flow in complex ways in complex structures. Transport of water and various organic and inorganic molecules in the central nervous system are important in a wide range of biological and medical processes [C. Nicholson, and S. Hrabetova, Biophysical Journal, 113(10), 2133(2017)]. However, the exact driving mechanisms are often not known. In this paper, we investigate flows induced by action potentials in an optic nerve as a prototype of the central nervous system (CNS). Different from traditional fluid dynamics problems, flows in biological tissues such as the CNS are coupled with ion transport. It is driven by osmosis created by concentration gradient of ionic solutions, which in term influence the transport of ions. Our mathematical model is based on the known structural and biophysical properties of the experimental system used by the Harvard group Orkand et al [R.K. Orkand, J.G. Nicholls, S.W. Kuffler, Journal of Neurophysiology, 29(4), 788(1966)]. Asymptotic analysis and numerical computation show the significant role of water in convective ion transport. The full model (including water) and the electrodiffusion model (excluding water) are compared in detail to reveal an interesting interplay between water and ion transport. In the full model, convection due to water flow dominates inside the glial domain. This water flow in the glia contributes significantly to the spatial buffering of potassium in the extracellular space. Convection in the extracellular domain does not contribute significantly to spatial buffering. Electrodiffusion is the dominant mechanism for flows confined to the extracellular domain.

SIGNIFICANCE The central nervous system ("brain") accumulates waste in tiny spaces between cells as thousands of signals move in billions of nerve cells every second. Potassium is dangerous waste because it can paralyze nerves and even kill them. Potassium moves as fluid flows and as it diffuses and migrates in electric fields. We describe glia, nerve cells, and extracellular space of optic nerves by unavoidable partial differential equations and show that potassium poisoning is prevented (mostly) by fluid flow through glia. We suggest that other wastes in the brain are removed by fluid flow through glia as part of the glymphatic system. Mathematics shows how glia pathways help 'cleanse the brain' so it can keep on working for many years.

1. Introduction

The now classical experiments of Hodgkin, Huxley, and Katz (1, 2) were designed to avoid the artifact of concentration polarization, the (significant) change of concentration of ions as the currents maintaining their voltage clamp flowed across electrodes inside the axon and its membranes. Change of concentration of potassium was seen nonetheless after a few milliseconds of outward potassium currents ((3): p. 482, 485, 489, 494; (4)), but the change was slow enough to be ignored in their calculations of the action potential (5).

The Kuffler group at Harvard was interested in the role of glia (6, 7) in the central nervous system and showed that the membrane potential of the optic nerve of ***Necturus*** reported the potassium concentration in the narrow extracellular space just outside axons, between glia and axon. Orkand et al (8) used this membrane potential of glia to report the change in potassium concentration—the polarization of concentration in the narrow extracellular space—as it accumulated during a train of nerve action potentials. Earlier work (3, 4) had inferred this concentration change. Orkand et al (7)

measured it quite directly. The artifact of concentration polarization that so worried Hodgkin and Huxley became the experimental reality of potassium accumulation (3) in the central nervous system (8), that interested the Kuffler group. Interest has only grown in the following fifty some odd years.

Potassium accumulation and flow in the extracellular space have been shown to have important roles in many papers focused on aging, Alzheimers disease, anesthesia, dementia, diabetes, epilepsy, migraine, sleep, stroke and traumatic brain injury. Potassium accumulation and flow play an important role in the biology of the central nervous system (9) normal, and abnormal (10–16). The glymphatic model has received much interest in the last months. It links potassium accumulation, flows in the extracellular space—particularly in sleep and diseases of aging—with general disposal of waste through glial pathways to the circulatory system (9, 17–21).

The accumulation of ions in a narrow extracellular space, like that between nerve and glia, or Schwann cell (4), depends on the diffusion, convection, and migration of ions in an electric field. Convection is likely to be important. Evolution uses the circulatory system to provide convective transport close to nearly every cell in a mammal, the lens of the eye being a notable exception, so the delays involved in electrodiffusion are overcome. Convection provides what diffusion denies: speed.

The optic nerve, and the mammalian central nervous system in general, involves nerve, glia and narrow extracellular space. It involves three types of flow, convection, diffusion, and migration in the electric field in radial and longitudinal directions of a cylindrical structure. It involves (chiefly) three ions (K, Na, Cl), and a number of different types of channels and pumps (voltage activated Na channels and at least two types of K channels and the Na/K pump). The description and analysis, not to say the numerical computation of the optic nerve, must deal with what is actually in the optic nerve. It must deal with what evolution has actually built in the central nervous system in general. Thus, the analysis must involve many forces, flows, structures, and channels and transporters. Here we report the subset of our work that deals with the accumulation of potassium in the narrow extracellular space of optic nerve.

The interactions between neuronal cells and glial cells have been included in models of the important phenomenon of spreading depression (22–25) thought to be related to epilepsy and migraine. Some two-compartment models for potassium clearance (or spatial buffering) include interactions between neuron cells and extracellular space (26) or interactions between glial cells and extracellular space (27–29). A tri-compartment model using ordinary differential equations (ODEs) was introduced by Sibille (30) to study the role of K_{ir4} channels. It shows that the flows play an important role in the central nerve system (31) via influx and efflux routes to help waste clearance, which has been called (with understandable enthusiasm if not hyperbole) a final frontier of neuroscience (32). Some models, including flow but not electrodiffusion, were introduced to study the pressure effect on the flow (33–36). Mori (15) proposed a multidomain model for cortical spreading depression, where ionic electrodiffusion and osmosis between different compartments are considered. In this paper, we first extend those results and the two-compartment structural analysis of the spherical lens (37) to the three-compartment cylindrical optic nerve fiber of ***Necturus***. Then we present some general conclusions based on the analysis of a specific set of experiments Orkand et al (7, 8) using a model distributed in space in both radial and longitudinal directions and that involves action potentials generated by Hodgkin Huxley equations.

This paper is organized as follows. The full model for microcirculation of water and ions are proposed based on conservation laws in Section 2. Then the model is calibrated and aligned with the Orkand experiment results in Section 3. In Section 4, the calibrated model is used to study the flow and ion microcirculations during Potassium clearance. A discussion on the parameters is presented in Section 5. Then the conclusions and future work are given in Section 6.

2. Mathematical model

In this section, we present a tridomain model for microcirculation of the optic nerve. The model deals with two types of flow: the circulation of water (hydrodynamics) and the circulation of ions (electrodynamics) in the

Journal Pre-proof

• glial compartment (Ω_{gl});

• axon compartment (Ω_{ax});

• extracellular space (Ω_{ex}).

The glial compartment and axon compartment exist only in the optic nerve, while extracellular space exists both in the optic nerve Ω_{ex}^{OP} and subarachnoid space Ω_{ex}^{SAS} (See Fig.1)

$$\Omega_{OP} = \Omega_{ax} \cup \Omega_{gl} \cup \Omega_{ex}^{OP}, \quad \Omega_{SAS} = \Omega_{ex}^{SAS}.$$

The model is mainly derived from laws of conservation of ions and water for flow through membranes between intracellular compartments and extracellular space (38).

Figure 1: Optic nerve structure. a: Key features of the optic nerve region and subarachnoid space (SAS); b: Longitudinal section of the optic nerve; c: cross section of the optic nerve.

Figure 2: Domain of the axial symmetry model. The optic nerve Ω_{OP} consist of axon compartment Ω_{ax}, glial compartment Ω_{gl} and extracellular space Ω_{ex}^{OP}. The subarachnoid space only has extracellular space Ω_{ex}^{SAS}. $R_a = 48\,\mu m$ is the radius of optic nerve and $R_b = 60\,\mu m$ is the radius from optical nerve center to the dura mater.

2.1. Notations and Assumptions

We first introduce the following notations used in the paper, where $i = \mathrm{Na}^+, \mathrm{K}^+, \mathrm{Cl}^-$ for ion species, $l = ex, gl, ax$ for extracellular space, glial compartment and axon compartment, and $k = gl, ax$ for glial or axon membrane in the optic nerve.

Fig.1 b shows the model with the whole domain Ω that consists of the subarachnoid space (SAS) region Ω_{SAS} and optic nerve region Ω_{OP} (see Fig.2),

$$\Omega = \Omega_{SAS} \cup \Omega_{OP}.$$

In the optic nerve region Ω_{OP}, the glial membrane and axon membrane separate domains Ω_{gl}, Ω_{ax} from the extracellular region Ω_{ex}^{OP}, respectively (also see Fig. 1). Based on the structure of the optic nerve, we have the following global assumptions for the model:

•Charge neutrality: In each domain, we assume that there is electroneutrality

$$\eta_{gl} \sum_i z^i C_{gl}^i + z^{gl} \eta_{gl}^{re} A_{gl} = 0, \qquad (1a)$$

$$\eta_{ax} \sum_i z^i C_{ax}^i + z^{ax} \eta_{ax}^{re} A_{ax} = 0, \qquad (1b)$$

$$\sum_i z^i C_{ex}^i = 0, \qquad (1c)$$

where $A_l > 0$ with $l = ax, gl$ is the density of proteins in axons or glial cells. The proteins are negatively charged, but the charge density is customarily described by a positive number. The η_{ax} and η_{gl} are the volume fraction of axon and glial compartments in the optic nerve and η_{ax}^{re} and η_{gl}^{re} are the resting state volume fractions.

Journal Pre-proof

•**Axial symmetry:** For simplicity, axial symmetry is assumed. The model can be straightforwardly extended to three dimensions when data and needs justify the considerable extra computational resources needed to analyze such models.

•**Isotropy of glial compartment and extracellular space:**

1) The extracellular space forms a narrow structure of branching clefts surrounding the glial cells and nerve axons.

2) The glial cells are connected to each other by connexins and form a syncytium.

3) The extracellular space is continuous and forms a syncytium.

Both syncytia are assumed isotropic here, until we know better. The axons are not connected to each other. For $l = gl, ex,$ and $i = \mathrm{Na}^+, \mathrm{K}^+, \mathrm{Cl}^-$, the ion flux and water flow velocity are in the following forms

$$\boldsymbol{j}_l^i = j_{l,r}^i \hat{\boldsymbol{r}} + j_{l,z}^i \hat{\boldsymbol{z}}, \qquad (2)$$

$$\boldsymbol{u}_l = u_l^r \hat{\boldsymbol{r}} + u_l^z \hat{\boldsymbol{z}}. \quad (3)$$

•**Anisotropy of axon compartment:** The axons are separated, more or less parallel cylindrical cells that do not form a syncytium. For $i = \mathrm{Na}^+, \mathrm{K}^+, \mathrm{Cl}^-$, the ion flux and water flow velocity are in the following forms

$$\boldsymbol{j}_{ax}^i = j_{ax,z}^i \hat{\boldsymbol{z}}, \qquad (4)$$

$$\boldsymbol{u}_{ax} = u_{ax}^z \hat{\boldsymbol{z}}. \qquad (5)$$

•**Communications between compartments:** The communications between intracellular compartments and extracellular space are through membranes. There is no direct interaction between glial and axon compartments. Interactions occur only through changes in concentration, electrical potential, and flows in the extracellular space (30).

The interface of optic nerve and SAS is the pia mater denoted by Γ_7,

$$\Omega_{OP} \bigcap \Omega_{SAS} = \Gamma_7.$$

In our model, both pia mater Γ_7 and dura mater Γ_4 are modeled as macroscopic membranes and appropriate boundary conditions. The transmembrane water flow through pia mater (39) depends on hydrostatic pressure, osmotic pressure and electric potential, while that through dura mater only depends on the hydrostatic pressure.

For the domain boundaries, Γ_1 is the radius center of the optic nerve; Γ_2 and Γ_3 are the far end (away from the eyeball) of the optic nerve which is connected to optic canal region (40). Γ_5 is used to model the dura mater connected to the sclera (the white matter of the eye) and assumed to be non-permeable (41). Γ_6 is used to denote the lamina cribrosa where the optic nerve head exits the eye posteriorly through pores of the lamina cribrosa (42).

2.2. Water circulation

We model water circulation with the following assumptions

• the loss or gain of water in axons and glial cells is only through membranes flowing into or out of the extracellular space.

• the transmembrane water flux is proportional to the intra/extra-cellular hydrostatic pressure and osmotic pressure differences.

• the glial cell and axons can swell and shrink due to the water inflows and outflows.

We use $\eta_l(r,z,t)$ to describe the volume fraction of *l* region $(l = gl, ax, ex)$, which varies over time and space due to transmembrane water flows. The conservation of water in each domain yields

$$\frac{\partial \eta_{gl}}{\partial t} + \mathcal{M}_{gl} U_{gl}^m + \nabla \cdot (\eta_{gl} \boldsymbol{u}_{gl}) = 0, \qquad (6a)$$

$$\frac{\partial \eta_{ax}}{\partial t} + \mathcal{M}_{ax} U_{ax}^m + \frac{\partial}{\partial z}(\eta_{ax} u_{ax}^z) = 0, \qquad (6b)$$

$$\nabla \cdot (\eta_{gl} \boldsymbol{u}_{gl}) + \nabla \cdot (\eta_{ex} \boldsymbol{u}_{ex}) + \frac{\partial}{\partial z}(\eta_{ax} u_{ax}^z) = 0, \qquad (6c)$$

where we use the fact that density of water is constant. Here $\boldsymbol{u}_l$ with $l = gl, ax, ex$ is the velocity in the glial cells, axons, and extracellular space, respectively. The transmembrane water flow U_k^m with $k = gl, ax$ follows the Starling's law on the *k*th membrane,

$$U_{gl}^m = L_{gl}^m \left(P_{gl} - P_{ex} - \gamma_{gl} k_B T (O_{gl} - O_{ex}) \right),$$

$$U_{ax}^m = L_{ax}^m \left(P_{ax} - P_{ex} - \gamma_{ax} k_B T (O_{ax} - O_{ex}) \right).$$

The P_l with $l = gl, ax, ex$ are the hydrostatic pressure in the glial cells, axons, and extracellular space, respectively. And $k_B T O_l$ is the osmotic pressure (37, 43) defined by

$$O_{ex} = \sum_i C_{ex}^i, \quad O_l = \sum_i C_l^i + A_l \frac{\eta_j^{re}}{\eta_l}, \quad l = gl, ax,$$

where $A_l \frac{\eta_l^{re}}{\eta_l} > 0$ is the density of the permanent negatively charged protein in glial cells and axons that varies with the volume (fraction) of the region. In this paper, we assume the permanent negatively charged protein is uniformly distributed within glial cells and axons and has valence z^l, $l = gl, ax$. The $\mathcal{M}_k$ and γ_k, $k = gl, ax$ are the glial cells (or axons) membrane area per unit volume and membrane reflection coefficient (44) respectively. L_{gl}^m and L_{ax}^m are the surface membrane hydraulic permeabilities of glial cells and axons. The membrane reflection coefficient γ_k $(k = gl, ax)$ is the ratio between the observed osmotic pressure and theoretical osmotic pressure. k_B is Boltzmann constant, and *T* is temperature.

For the volume fraction $\eta_l, l = gl, ax, ex$, we have

$$\eta_{gl} + \eta_{ax} + \eta_{ex} = 1, \quad \text{in } \Omega. \qquad (7)$$

Remark 2.1.

Note the glial cells and axons are found only in the Ω_{OP} region. In other words, $\eta_{ax} = \eta_{gl} \equiv 0$ and $\eta_{ex} \equiv 1$ are fixed in Ω_{SAS}. Therefore, the solution is incompressible in the Ω_{SAS}, and we have

$$\nabla \cdot \boldsymbol{u}_{ex} = 0, \quad \text{in } \Omega_{SAS}. \qquad (8)$$

Journal Pre-proof

The relation between the hydrostatic pressure P_l and volume fraction $\eta_l\ (l = gl, ax, ex)$ is connected by the force balance on the membrane $\mathcal{M}_k\ (k = gl, ax)$. The membrane force is balanced with the hydrostatic pressure difference on both sides of the semipermeable membrane (15, 43). Then the variation of volume fraction from the resting state is proportional to the variation of hydrostatic pressure difference from the resting state.

$$K_{gl}\left(\eta_{gl}-\eta_{gl}^{re}\right)=P_{gl}-P_{ex}-\left(P_{gl}^{re}-P_{ex}^{re}\right), \qquad (9a)$$

$$K_{ax}\left(\eta_{ax}-\eta_{ax}^{re}\right)=P_{ax}-P_{ex}-\left(P_{ax}^{re}-P_{ex}^{re}\right), \qquad (9b)$$

where $K_{gl,ax}$ is the stiffness constant and η_l^{re} and $P_l^{re}\ (l = gl, ax, ex)$ are the resting state volume fraction and hydrostatic pressure.

Remark 2.2.

*The osmotic pressure influences the volume fraction in an implicit way. Due to Eq. (*6*) and the definition of transmembrane water flow* U_{gl}^{m}*, the osmostic pressure difference induces the transmembrane water flow going in and out of compartments, and the hydrostatic pressure changes correspondingly.*

Remark 2.3.

In reality, both dura mater Γ_7 *and pia mater* Γ_4 *are deformable. However, the stiffness of them are much larger than glial cells'* (45–47)*. For the sake of simplicity, we neglect the deformation of dura mater and pia mater so the system could be solved in fixed domains* Ω *and* Ω^{OP}*. We are aware that in some important clinical applications the deformation is of great importance and that our model will need to be extended to deal with them. The extensions do not produce analytical challenges but they are likely to add significant complexity to the numerical methods and make the computations much more involved and longer.*

Note that the concentrations of ions and effective concentration of water vary a great deal and so are described by equations in which the number density of ions and effective number density of water vary in both the radial and longitudinal directions according to conservation laws, without using compartments that may not have unique definitions or relations to anatomical structures. Indeed, the variation of concentration is one of the main determinants of the properties of ionic solutions. The solution is incompressible, the components are not (48).

Next, we define the velocity in each domain.

Water Velocities in the Glial Compartment. As we mentioned before, the glial cells are connected through the narrow connections on the membranes and form a syncytium. The fluid velocity inside the compartment is limited by the transmembrane fluid velocity, which is determined by the difference of hydro pressure and osmotic pressure on both sides of the membrane (15, 43). On the macro-scale, by using averaging process (37, 49, 50), the glial compartment is treated with membranes everywhere. So the velocity of fluid in glial syncytium $\boldsymbol{u}_{gl}$ depends on the gradients of hydrostatic pressure and osmotic pressure:

$$u_{gl}^{r}=-\frac{\kappa_{gl}\tau_{gl}}{\mu}\left(\frac{\partial P_{gl}}{\partial r}-\gamma_{gl}k_{B}T\frac{\partial O_{gl}}{\partial r}\right), \qquad (10a)$$

$$u_{gl}^{z}=-\frac{\kappa_{gl}\tau_{gl}}{\mu}\left(\frac{\partial P_{gl}}{\partial z}-\gamma_{gl}k_{B}T\frac{\partial O_{gl}}{\partial z}\right). \qquad (10b)$$

Substituting Eq. (10a) into the incompressibility (6a) yields a Poisson equation for pressure in the glial compartment. The boundary conditions in the glial syncytium are as follows

$$\begin{cases} \dfrac{\partial P_{gl}}{\partial r} = 0, & \text{on } \Gamma_1 \cup \Gamma_7, \\ \dfrac{\partial P_{gl}}{\partial z} = 0, & \text{on } \Gamma_2 \cup \Gamma_6, \end{cases} \tag{11}$$

where homogeneous Neumann boundary condition is applied at all four of these boundaries.

Water Velocity in the Axon Compartment. Axons are arranged parallel in the longitudinal direction and are isolated from each other. The fluid velocity in the axon compartment is defined along *z* direction as

$$u_{ax}^{r} = 0, \tag{12a}$$

$$u_{ax}^{z} = -\frac{\kappa_{ax}}{\mu}\frac{\partial P_{ax}}{\partial z}. \tag{12b}$$

Similarly, substituting above velocity into the incompressibility equation gives the Poisson equation for pressure in the axon compartment. A homogeneous Neumann condition for pressure is used on the left and right boundaries of the axon compartment

$$\frac{\partial P_{ax}}{\partial z} = 0, \text{ on } \Gamma_2 \cup \Gamma_6. \tag{13}$$

Velocity in the Extracellular Space. The extracellular space is a narrow connected domain, where the electro-osmotic effect needs to be considered (37, 51, 52). The extracellular velocity is determined by the gradients of hydrostatic pressure and electric field

$$u_{ex}^{r} = -\frac{\kappa_{ex}\tau_{ex}}{\mu}\frac{\partial P_{ex}}{\partial r} - k_e\tau_{ex}\frac{\partial \phi_{ex}}{\partial r}, \tag{14a}$$

$$u_{ex}^{z} = -\frac{\kappa_{ex}\tau_{ex}}{\mu}\frac{\partial P_{ex}}{\partial z} - k_e\tau_{ex}\frac{\partial \phi_{ex}}{\partial z}, \tag{14b}$$

where ϕ_{ex} is the electric potential in the extracellular space, τ_{ex} is the tortuosity of extracellular region (38, 53) and μ is the viscosity of water, k_e describes the effect of electro-osmotic flow (51, 52, 54), κ_{ex} is the permeability of the extracellular space. Here the hydro permeability κ_{ex}, tortuosity τ_{ex} and electric-osmotic parameter k_e have two distinguished values in the region Ω_{ex}^{OP} and Ω_{ex}^{SAS},

$$\kappa_{ex} = \begin{cases} \kappa_{ex}^{OP}, \text{ in } \Omega_{OP}, \\ \kappa_{ex}^{SAS}, \text{ in } \Omega_{SAS}, \end{cases} \quad \tau_{ex} = \begin{cases} \tau_{ex}^{OP}, \text{ in } \Omega_{OP}, \\ \tau_{ex}^{SAS}, \text{ in } \Omega_{SAS}, \end{cases} \tag{15}$$

$$k_e = \begin{cases} k_e^{OP}, \text{ in } \Omega_{OP}, \\ k_e^{SAS}, \text{ in } \Omega_{SAS}, \end{cases}$$

Remark 2.4.

*By substituting the definitions of velocities Eqs. (*12a*), (*10a*) and (*14a*), and volume fractions Eq.(*9a*) into the mass conservation law Eq. (*6*), it yields the evolution equations of hydrostatic pressure in different compartments, which are solved during the simulations in Session* 4*.*

Since $\Gamma_2 \cup \Gamma_3$ are the far end of optic nerve away from eyeball and connect to the optic canal, we assume the hydrostatic pressure of extracellular fluid is equal to the cerebrospinal fluid pressure. On the other hand, the intraocular pressure (IOP) is imposed at Γ_6 where the extracellular space is

connected to the retina. At the boundary Γ_5, we assume a non-permeable boundary. We are aware of the significance of the pressures and flows at these boundaries for clinical phenomena including glaucoma (36, 55, 56) and will return to that subject in later publications.

The water flow across the semi-permeable membrane Γ_4 is produced by the lymphatic drainage on the dura membrane, which depends on the difference between extracellular pressure and orbital pressure (OBP). We assume the velocity across the pia membrane Γ_4, is continuous and determined by the hydrostatic pressure and osmotic pressure. To summarize, the boundary conditions of the extracellular fluid are

$$\begin{cases} \boldsymbol{u}_{ex}\cdot\hat{\boldsymbol{r}}=0, & \text{on } \Gamma_1,\\ P_{ex}=P_{CSF}, & \text{on } \Gamma_2\cup\Gamma_3,\\ \boldsymbol{u}_{ex}^{SAS}\cdot\hat{\boldsymbol{r}}=L_{dr}^{m}\left(P_{ex}^{SAS}-P_{OBP}\right), & \text{on } \Gamma_4,\\ \boldsymbol{u}_{ex}\cdot\hat{\boldsymbol{z}}=0, & \text{on } \Gamma_5,\\ P_{ex}=P_{IOP}, & \text{on } \Gamma_6,\\ \boldsymbol{u}_{ex}^{OP}\cdot\hat{\boldsymbol{r}}=\boldsymbol{u}_{ex}^{SAS}\cdot\hat{\boldsymbol{r}} & \\ =L_{pia}^{m}\left(P_{ex}^{OP}-P_{ex}^{SAS}-\gamma_{pia}k_BT\left(O_{ex}^{OP}-O_{ex}^{SAS}\right)\right), & \text{on } \Gamma_7, \end{cases} \tag{16}$$

where P_{CSF} is the cerebrospinal fluid pressure (36) and P_{IOP} is the intraocular pressure and P_{OBP} is the orbital pressure on the dura mater.

2.3. Ion Transport

For ion circulation, we assume

• only three types of ions are considered: $\mathrm{Na}^+, \mathrm{K}^+$ and Cl^-.

• the sodium-potassium ATP pump is present on both glial and axon membranes.

• ion channel conductance on glial cell membranes is a fixed constant, independent of the voltage and time. The sodium conductance is assumed small, and its channel origin unknown. The potassium conductance is large and comes from the K_{ir4} channels (31, 57). When experimental evidence is available, other types of pumps and channels can be added to the model.

• sodium channel and potassium channel conductance on axons are voltage-gated, while the conductance of chloride channel is fixed.

The conservation of ions implies the following system of partial differential equations to describe the dynamics of ions in each region, for $i=\mathrm{Na}^+,\mathrm{K}^+,\mathrm{Cl}^-$

$$\frac{\partial\left(\eta_{gl}C_{gl}^{i}\right)}{\partial t}+\mathcal{M}_{gl}J_{gl}^{m,i}+\nabla\cdot\left(\eta_{gl}\boldsymbol{j}_{gl}^{i}\right)=0, \tag{17a}$$

$$\frac{\partial\left(\eta_{ax}C_{ax}^{i}\right)}{\partial t}+\mathcal{M}_{ax}J_{ax}^{m,i}+\frac{\partial}{\partial z}\left(\eta_{ax}j_{ax,z}^{i}\right)=0, \tag{17b}$$

$$\frac{\partial\left(\eta_{ex}C_{ex}^{i}\right)}{\partial t}-\mathcal{M}_{ax}J_{ax}^{m,i}-\mathcal{M}_{gl}J_{gl}^{m,i}+\nabla\cdot\left(\eta_{ex}\boldsymbol{j}_{ex}^{i}\right)=0, \tag{17c}$$

where the last equation reduces to the following in the Ω_{SAS} region,

Journal Pre-proof

$$\frac{\partial C_{ex}^{i,SAS}}{\partial t}+\nabla\cdot \boldsymbol{j}_{ex}^{i,SAS}=0. \quad (18)$$

The transmembrane ion flux $J_k^{m,i}\,(k=gl,ax)$ consists of active ion pump source a_k^i and passive ion channel source b_k^i, for ion *i* on the axons $(k=ax)$ or glial cells membranes $(k=gl)$. In the glial cell membranes,

$$J_k^{m,i}=a_k^i+b_k^i,\quad k=gl,ax,\quad i=\mathrm{Na}^+,\mathrm{K}^+,\mathrm{Cl}^-.$$

In the glial cell membranes, b_{gl}^i is defined as

$$b_{gl}^i=\frac{g_{gl}^i}{z^i e}\left(\phi_{gl}-\phi_{ex}-E_{gl}^i\right), \quad (19)$$

where the Nernst potential is used to describe the gradient of chemical potential $E_{gl}^i=\frac{k_B T}{ez^i}\log\left(\frac{C_{ex}^i}{C_{gl}^i}\right)$ and the conductance g_{gl}^i for each ion on the glial membrane is a fixed constant, independent of voltage and time. On the axon's membrane, b_{ax}^i is defined as

$$b_{ax}^i=\frac{g_{ax}^i}{z^i e}\left(\phi_{ax}-\phi_{ex}-E_{ax}^i\right), \quad (20)$$

where

$$g_{ax}^{Na}=\bar{g}^{Na}m^3h+g_{leak}^{Na},\quad g_{ax}^{K}=\bar{g}^{K}n^4+g_{leak}^{K},$$
$$E_{ax}^i=\frac{k_B T}{ez^i}\log\left(\frac{C_{ex}^i}{C_{ax}^i}\right).$$

The time-dependent dynamic of open probability, often loosely called 'gating' is governed by the Hodgkin-Huxley model (58, 59)

$$\frac{dn}{dt}=\alpha_n(1-n)-\beta_n n, \quad (21a)$$

$$\frac{dm}{dt}=\alpha_m(1-m)-\beta_m m, \quad (21b)$$

$$\frac{dh}{dt}=\alpha_h(1-h)-\beta_h h. \quad (21c)$$

We assume that the only pump is the Na/K active transporter. We are more than aware that other active transport systems can and likely do move ions and water in this system. They will be included as experimental information becomes available.

In the case of the Na/K pump $a_l^i, l=ax,gl$, the strength of the pump depends on the concentration in the intracellular and extracellular space (59, 60), i.e.

$$a_k^{Na}=\frac{3I_k}{e}, a_k^K=-\frac{2I_k}{e}, a_k^{Cl}=0, k=gl,ax, \quad (22)$$

where

Journal Pre-proof

$$I_k = I_{k,1}\left(\frac{c_k^{Na}}{c_k^{Na}+K_{Na1}}\right)^3\left(\frac{c_{ex}^{K}}{c_{ex}^{K}+K_{K1}}\right)^2 + I_{k,2}\left(\frac{c_k^{Na}}{c_k^{Na}+K_{Na2}}\right)^3\left(\frac{c_{ex}^{K}}{c_{ex}^{K}+K_{K2}}\right)^2,$$

$I_{k,1}$ and $I_{k,2}$ are related to α_1- and α_2- isoform of $\mathrm{Na/K}$ pump.

The definitions of ion flux in each domain are as follows, for $i=\mathrm{Na}^+,\mathrm{K}^+,\mathrm{Cl}^-$,

$$\boldsymbol{j}_l^i = C_l^i\boldsymbol{u}_l - D_l^i\tau_l\left(\nabla C_l^i + \frac{z^i e}{k_B T}C_l^i\nabla\phi_l\right), l=gl,ex, \qquad (23a)$$

$$j_{ax,z}^i = C_{ax}^i u_{ax}^z - D_{ax}^i\left(\frac{\partial C_{ax}^i}{\partial z}+\frac{z^i e}{k_B T}C_{ax}^i\frac{\partial\phi_{ax}}{\partial z}\right). \qquad (23b)$$

For the axon compartment boundary condition, we have

$$C_{ax}^i = C_{ax}^{i,re}, \quad \text{on}\ \Gamma_2\bigcup\Gamma_6,$$

and

$$\begin{cases}\dfrac{\partial C_{gl}^i}{\partial r}=0, & \text{on}\ \Gamma_1,\\ C_{gl}^i = C_{gl}^{i,re}, & \text{on}\ \Gamma_2\bigcup\Gamma_6,\\ \boldsymbol{j}_{gl}^i\cdot\hat{\boldsymbol{r}}=0, & \text{on}\ \Gamma_7,\end{cases}$$

where the Dirichlet boundary conditions are used at locations $\Gamma_2\bigcup\Gamma_6$ for axons and glial cell, and a non-flux boundary condition is used for glial cells ions flux on the radius center Γ_1 and pia mater Γ_7 .

For the extracellular space boundary condition, similar boundary conditions are imposed except on the pia mater Γ_7. The flux across the pia mater is assumed continuous and Ohm's law is used (37). Additionally, a non-permeable boundary condition is used at location Γ_5 and a homogeneous Neumann boundary condition is applied at the location of the dura mater Γ_4,

$$\begin{cases}\dfrac{\partial C_{ex}^i}{\partial r}=0, & \text{on}\ \Gamma_1,\\ C_{ex}^i = C_{csf}^i, & \text{on}\ \Gamma_2\bigcup\Gamma_3,\\ \dfrac{\partial C_{ex}^i}{\partial r}=0, & \text{on}\ \Gamma_4,\\ \boldsymbol{j}_{ex}^i\cdot\hat{\boldsymbol{z}}=0, & \text{on}\ \Gamma_5,\\ C_{ex}^i = C_{IOP}^i, & \text{on}\ \Gamma_6,\\ \boldsymbol{j}_{ex}^{i,OP}\cdot\hat{\boldsymbol{r}} = \boldsymbol{j}_{ex}^{i,SAS}\cdot\hat{\boldsymbol{r}} = \dfrac{G_{pia}^i}{z^i e}\left(\phi_{ex}^{OP}-\phi_{ex}^{SAS}-E_{pia}^i\right), & \text{on}\ \Gamma_7.\end{cases} \qquad (24)$$

Journal Pre-proof

Multiplying equations in (17a-17c) with $z_i e$ respectively, summing up, and using equation (1a-1c) and equations (23), we have following system for the electric potential in ax, gl, ex

$$\sum_i z^i e \mathcal{M}_{gl} J_{gl}^{m,i} + \sum_i \nabla \cdot \left(z^i e \eta_g \boldsymbol{j}_{gl}^i \right) = 0, \quad \text{(25a)}$$

$$\sum_i z^i e \mathcal{M}_{ax} J_{ax}^{m,i} + \sum_i \frac{\partial}{\partial z} \left(z^i e \eta_{ax} j_{ax,z}^i \right) = 0, \quad \text{(25b)}$$

$$\sum_i \nabla \cdot \left(z^i e \eta_{gl} \boldsymbol{j}_{gl}^i \right) + \sum_i \frac{\partial}{\partial z} \left(z^i e \eta_{ax} j_{ax,z}^i \right) + \sum_i \nabla \cdot \left(z^i e \eta_{ex} \boldsymbol{j}_{ex}^i \right) = 0, \quad \text{(25c)}$$

which describe the spatial distributions of electric potentials in three compartments.

In the subarachnoid space Ω_{SAS}, the governing equation for extracellular electric potential reduces to

$$\nabla \cdot \left(\sum_i z^i e \boldsymbol{j}_{ex}^{i,SAS} \right) = 0. \quad \text{(26)}$$

The boundary conditions for electric fields ϕ_{ax}, ϕ_{gl} and ϕ_{ex} are given below.

In the axon compartment:

$$\begin{cases} \dfrac{\partial \phi_{ax}}{\partial z} = 0, & \text{on } \Gamma_2, \\ \dfrac{\partial \phi_{ax}}{\partial z} = 0, & \text{on } \Gamma_6, \end{cases}$$

In the glial compartment:

$$\begin{cases} \dfrac{\partial \phi_{gl}}{\partial r} = 0, & \text{on } \Gamma_1, \\ \dfrac{\partial \phi_{gl}}{\partial z} = 0, & \text{on } \Gamma_2, \\ \dfrac{\partial \phi_{gl}}{\partial z} = 0, & \text{on } \Gamma_6, \\ \dfrac{\partial \phi_{gl}}{\partial r} = 0, & \text{on } \Gamma_7, \end{cases}$$

and in the extracellular space:

Journal Pre-proof

$$
\begin{cases}
\dfrac{\partial \phi_{ex}}{\partial r} = 0, & \text{on } \Gamma_1, \\
\dfrac{\partial \phi_{ex}}{\partial z} = 0, & \text{on } \Gamma_2 \cup \Gamma_3, \\
\dfrac{\partial \phi_{ex}}{\partial r} = 0, & \text{on } \Gamma_4, \\
\dfrac{\partial \phi_{ex}}{\partial z} = 0, & \text{on } \Gamma_5, \\
\dfrac{\partial \phi_{ex}}{\partial z} = 0, & \text{on } \Gamma_6, \\
\sum_i z^i e \boldsymbol{j}_{ex}^{i,OP} \cdot \hat{\boldsymbol{r}} = \sum_i z^i e \boldsymbol{j}_{ex}^{i,SAS} \cdot \hat{\boldsymbol{r}} & \\
= \sum_i G_{pia}^i \left(\phi_{ex}^{OP} - \phi_{ex}^{SAS} - E_{pia}^i \right), & \text{on } \Gamma_7.
\end{cases}
\tag{27}
$$

3. Model calibration

Our work is possible because of, and was motivated by the paper of Orkand et al (7, 8) that measured the accumulation of potassium in the narrow extracellular space (Ω_{ex}^{OP}) of the optic nerve of the amphibian salamander Necturus, in the spirit of the original work of Frankenhaeuser and Hodgkin (4), that first identified and analyzed accumulation of potassium outside a nerve fiber. The existence and qualitative properties of that accumulation of potassium were known to, and a cause for concern for Hodgkin, from his first work on the voltage clamp (1, 2), if not earlier. Hodgkin described the phenomena as part of what was called [concentration] 'polarization' and discussed it extensively with students sometime later (Eisenberg, personal communication, 1962)

The key experiment in the Orkand paper (8) measures the change in potential across the glial membrane produced by a train of action potentials. The glial membrane potential is used to estimate and report the potassium concentration in the narrow extracellular space, because the glial membrane is populated with more or less voltage independent potassium channels and not much else.

In the experiment, optic nerve has been put in three different K^+ concentrations (1.5 mM, 3 mM, 4.5 mM) in the bathing solution to change the resting potential across the glia membrane. Then the axon was stimulated to give a train of action potentials. The action potentials increased K^+ in Ω_{ex}^{OP} . The accumulated K^+ then made the glia membrane potential more positive. Stimuli were applied at both ends of a region of the optic nerve thereby producing a more uniform (in space) potential within that region.

The model of this system is solved by using the Finite Volume Method with mesh size $h = 1/20$ and temporal size $t = 1/10$ in dimensionless units. The code is written and executed in the Matlab environment. The flowchart for the simulation is shown in Fig. 3. In the first step, we obtain the resting state of the system by iteration and fixed volume fraction (7)

$$\eta_{ax}^{re} = 0.5, \eta_{gl}^{re} = 0.4, \eta_{ex}^{re} = 0.1.$$

In the dynamic process, the resting state values are taken as initial values. Then, we first solve the concentration governing equations, followed by electrical potentials equation and pressure equations. We update the volume fraction by using Eqs. (9a) and (9b).

Figure 3: Flowchart for simulation process

Journal Pre-proof

In our simulation study, we first set the ECS (Ω_{ex}^{OP}) concentration of K^+ to be 3mM and obtained a resting potential across the glial membrane $(\sim -89\,\text{mV})$. In Orkand's work (7, 8), suction electrodes were used for stimulating; The two ends of the optic nerve were placed in suction electrodes as described in their Methods Section. We modeled the suction electrodes by applying a train of rectangular function (sometimes called a 'box car' stimulus in the engineering literature) currents through the axon membrane at $z = 2.25\,\text{mm}, 13.5\,\text{mm}, \text{and}\, 0 < r < R_a = 48\,\mu m$. Each stimulus in the train lasted 3ms (as Orkand's paper indicated) with current strength $3\text{mA}/\text{m}^2$. The stimulus was large enough to exceed the threshold and generate action potentials. After a train of stimuli with a frequency of $17/\text{s}$ for $1\ \text{s}$, the first panel of Figure 4 shows the train of axon membrane action potentials and its return to the initial level $(\sim -89\,\text{mV})$ after 1s. The profiles of the first action potential and the last action potential in the train are presented in the second panel. The third and fourth panels are used to illustrate the increase in glial cell membrane potential and extracellular potassium concentration during and after the train of stimuli. The fourth panel of Figure 4 shows that during stimulus, the K^+ concentration in Ω_{ex}^{OP} keeps increasing due to the opening of the voltage-gated potassium channel of the axon membrane. As a result of the accumulated K^+ in Ω_{ex}^{OP}, the membrane potential of glial cells also continues to increase until the stimulus stops.

Figure 4: Recording axon membrane potential, glial membrane potential and extracellular K^+ at center axis point (where $r = 0$ and $z = L/2$) when the extracellular solution with 3mM K^+. Then, we vary the K^+ to be 1.5 mM, 3 mM, 4.5 mM in Ω_{ex}^{OP} and record the magnitude of the maximum glial membrane depolarized potential in each case as in the Fig. 5. The black symbols are used for experimental data, red ones are the simulations results of our model, respectively. Fig. 5 shows that our model could match the experimental resting potentials (solid symbols) and depolarization potentials (open symbols) very well with different K^+ concentrations in Ω_{ex}^{OP}.

Our work is limited by the lack of other types of data for calibration, although it is important to remember that the structural parameters, values of membrane capacitance, many conductance variables, and resistivities of bulk solutions are known quite well because of the work of generations of anatomists, physiologists, and biophysicists.

Figure 5: Comparison between the experiment in (8) and simulation on the effect of nerve impulses on the membrane potential of glial cells. The solid symbols are resting potentials and the open symbols are depolarization potentials with different K^+ concentrations in Ω_{ex}^{OP}.

4. Potassium clearance

In this section, we compare the potassium clearance under various conditions based on the full model. In Section 4.1, by applying the stimuli at alternative locations on the axon, we show how the interaction between the extracellular pathway and glial transmembrane pathway helps potassium clearance. The microcirculation patterns of water and ions between glial compartment and extracellular space is presented. In Section 4.2, we have a glimpse of the effect of the glial membrane conductance changes as well as variations in the pia mater boundary conditions. We introduce the NKCC channel into the glial membrane and a non-selective pathway on the pia mater and compare the potassium clearance with the baseline model. The NKCC channels on the glial membrane increase potassium clearance efficiency. An additional non-selective pathway in the pia mater does not have significant effect on potassium clearance due to the limited surface area of pia mater.

4.1. Alternative Distribution of Stimulus Location

In this section, current is applied at several different radial locations. We wondered whether the choice of radial location would change our calculations of potassium clearance and fluid velocity.

Journal Pre-proof

This approach is used for many variables to crudely estimate the sensitivity of our results to assumptions.

To facilitate the discussion of the interaction between the extracellular pathway and the glial transmembrane pathway for K^+ clearance, we define the following regions which potassium flux could pass through,

- M_S : Glial membrane in stimulated region,
- E_T : Extracellular pathway on transition interface.
- M_{NS} : Glial transmembrane in non-stimulated region.
- G_T : Glial pathway on transition interface.

The normal directions on M_S and M_{NS} point to extracellular space and the normal direction of E_T and G_T is the radial direction. We mainly focus on the two particular periods of time, (1) during a train of axon firing $([0, T_{sti}])$ (2) after axon firing $([T_{sti}, T_{af}])$ after the axon stimulation stops. In the simulations below, we take $T_{sti} = 0.2\,\mathrm{s}$ and $T_{af} = 10\,\mathrm{s}$. The frequency of the stimuli is $50\,\mathrm{Hz}\,(T = 0.02\,\mathrm{s})$ and each single stimulus has current strength $I_{sti} = 3\times10^{-3}\,\mathrm{A/m^2}$ with duration $3\,\mathrm{ms}$.

4.1.1. Inner and Outer radial regions stimulated

We first make a comparison between the inner radial region stimulated case in which the current is applied at $z = z_0\,(= 2.25\,\mathrm{mm})$ cross-section: $S_{sti}^{in}(=\{(r,z)\,|\,r < \frac{R_a}{2}, z = z_0\})$ and outer radial region stimulated case in which $S_{sti}^{out}(=\{(r,z)\,|\,\frac{R_a}{2} < r < R_a, z = z_0\})$. Since the axon signal propagates in the *z* direction, for the inner radial region stimulated case, the stimulated region is $V_S^{in} = \{(r,z)\,|\,r < \frac{R_a}{2}, z \in [0, L]\}$ and the non-stimulated region is $V_{NS}^{in} = \{(r,z)\,|\,\frac{R_a}{2} < r < R_a, z \in [0, L]\}$; for the outer radial region stimulated case, $V_S^{out} = V_{NS}^{in}$ and $V_{ns}^{out} = V_s^{in}$. The transition interface $S_{sti} = \{(r,z)\,|\,r = \frac{R_a}{2}, z \in [0, L]\}$ is the same for both cases.

(a) During a train of neuron firing

In Fig. 6, we show the total potassium flux (potassium flux density integrated over area) and cumulative potassium flux (total potassium flux integrated over time) during the axon firing period $[0, T_{sti}]$. In both cases, the figures show that the transmembrane flow from extracellular to glial and the communication inside the extracellular act together to help the potassium clearance. The strength of fluxes is gradually increased during axon firing period as in Fig. 6a & b. The results confirm that the potassium flux during stimulus flows from the stimulus region to the non-stimulus region, in both the extracellular space and glial compartment. The cumulative potassium flux through the glial membrane (M_S) is twice as large as that through the extracellular pathway in the transition interface (E_T) as shown in Fig. 6e&f.

Figure 6: a-d: Potassium flux through M_S, E_T, M_{NS} and G_T during a train of axon firing. e-h: cumulative potassium flux during axon firing period $[0, T_{sti}]$.

Journal Pre-proof

The glial compartment serves as an important and quick potassium transport device to remove potassium accumulated while the neuron fires action potentials. In the stimulated region, the accumulated potassium makes the potassium Nernst potential more positive. The change in the potassium Nernst potential induces potassium movement into the glial compartment from the extracellular space (Fig. 6a). This inflow makes the glial compartment electric potential more positive and moves potassium ions from the stimulated region to the unstimulated region (Fig. 6d). In the unstimulated region, the glial membrane potential also becomes more positive as it does in the stimulated region, because the glia is an electrical syncytium in the longitudinal and radial directions. However, the glial potassium Nernst potential in the unstimulated region is not very different from that in the resting state. These potentials produce the outward potassium flux from the glial compartment in the unstimulated region (Fig. 6c). Interacting regions of this sort depend on spatial variables and the properties of the glia as a syncytium in the longitudinal as well as radial directions. It is difficult to capture these effects in models that do not include radial and longitudinal directions as independent variables. Compartment models are possible but it is very difficult to uniquely define invariant parameters over the range of conditions of interest. If additional information becomes available experimentally, the "new" conductances and pumps cannot be introduced in a unique way, without much thought. As the model is adapted to other structures in the brain, the parameters of a compartment model become quite difficult to specify. The distributed model uses structurally defined parameters with structural or specific biophysical meaning. These can be adjusted in a reasonably specific way in different versions of this model, appropriate for different systems in the brain. The schematic graph of potassium circulation in the optic nerve is summarized in the Fig. 10a.

The spatial distributions of K^+ concentration changes from resting state over time are shown in the Fig. 7 and Fig. 8. Fig. 7 shows that the K^+ concentration varies in the stimulus region along the longitudinal direction during one action potential, while there is no change of K^+ in the non-stimulus region. Fig. 8 a & b show there an obvious potassium concentration difference in the radial direction after a train of stimuli over time $T_{sti} = 0.2s$. In Fig. 8c, the potassium concentration difference vanishes due to the communication of the extracellular space and glial compartment shown in Fig 11fg.

Figure 7: Spatial distribution of potassium changes from the resting state during an action potential.

Figure 8: Spatial distribution of potassium changes from the resting state during and after a train of stimuli.

Figure 9: a-d: Average water velocity through M_S, E_T, M_{NS} and G_T during a train of axon firing period $[0, T_{sti}]$. e-f: the extracellular volume fraction variation in the stimulated region and non-stimulated region.

Figure 10: a: Schematic graph of the potassium flux when axon is stimulated. In the stimulated region, the potassium moves through the extracellular pathway and through the glial compartment by way of the glial membrane. In the non-stimulated region, the potassium leaks out to the extracellular space through the glial membrane. b: Schematic graph of the water circulation when the inner part of the axon is stimulated. In the stimulated region, the glial transmembrane water flow goes from extracellular space into glial compartment as the effect of osmosis difference. In the extracellular space, water goes from non-stimulated region to stimulated region in the radial direction. In the glia compartment goes in the opposite direction. Note these graphs summarize outputs of large numbers of calculations solving partial differential equations in longitudinal and radial spatial directions and time. They do not represent a compartmental model. They are the output of a model distributed in space.

The water circulation in the optic nerve is driven by the gradient of osmotic pressure in the stimulated region. In the stimulated region, the extracellular osmotic pressure $k_B TO_{ex}$ decreased, and glial compartment osmotic flow of water is increased. This is because there is more potassium flux moving into the glial compartment through the glial membrane, but a smaller amount of sodium flux out of

Journal Pre-proof

the glial compartment because of the ion channel conductance difference between the potassium and sodium channels in the glial membrane. In the glial compartment in the stimulated region of the optic nerve fiber, there is an increase in the water flux into the glial compartment from the extracellular space (Fig. 9a). The volume fraction of the glial compartment and the hydrostatic pressure have also increased. The increased hydrostatic pressure in the stimulated region also raises the hydrostatic pressure in locations far away from the stimulated region. The increased pressure also drives the flow from stimulated region to the unstimulated region because the glial compartment is a connected space (Fig. 9d), a longitudinal syncytium. In the unstimulated region, the water flows out of the glial compartment into the unstimulated region because of the increased hydrostatic pressure in the glial compartment (Fig 9c). Then, because the fluid is incompressible, the fluid in the unstimulated region flows back to the stimulated region (Fig. 9b). The schematic graph of water circulation in the optic nerve is summarized in Fig. 10b. This is a summary of our results. It is not a compartment model. Our models are distributed.

In Fig. 9e&f, we show the volume change of extracellular space. In the stimulated region, the extracellular space decreases because the water flows into the glial cell; while in the unstimulated region, the extracellular space swells because of spatial buffering water flow (61).

In sum, during a train of action potentials in the axon, the potassium flux transport pattern and potassium flux strength across the glia membrane and through the extracellular pathway are the same for both radial regions, inner and outer. The glial compartment pathway is the dominant clearance mechanism of the potassium accumulated in the extracellular stimulated region, in both cases.

(b) After axon firing period

After the stimulus period, the main potassium clearance mechanism is the passive flow from extracellular space to glial compartment through the glial membrane. The potassium flux in extracellular region and glial compartment is negligible. In these calculations, the extracellular region and the glial compartment could be approximated as a single compartment. We show a schematic figure of potassium flux pattern in Fig. 13a. This is a summary and sketch of our results. We did not use a compartment model. Our model is distributed.

Figure 11: a-d: potassium flux through M_S, E_T, M_{NS}, and G_T after a train action potentials. e-h: cumulative potassium flux after axon firing.

In the Fig. 11, we show the total potassium flux and cumulative potassium flux through M_S, E_T, M_{NS}, and G_T after axon firing period $[T_{sti}, T_{af}]$. For both cases, the strength of potassium fluxes through the glial transmembrane pathway (M_S) and extracellular pathway have dramatically decreased after the axon stopped firing.

Fig. 11e shows that in both cases (inner stimulus and outer stimulus), the potassium flows into the stimulated glial compartment after the axon firing period. Fig. 11g shows that the potassium flux through the glial membrane in the non-stimulated region reverses its direction for a short time after axon stop firing. This occurs because the extracellular potassium concentration becomes evenly distributed in both the stimulated and non-stimulated extracellular space.

Figure 12: a-d: Average water velocity through M_S, E_T, M_{NS} and G_T after a train of axon firing.

Figure 13: a: Schematic graph of the potassium flux after the axon was stimulated. The potassium flux leaks into the glial compartment from the extracellular space through the glial membrane in both stimulated and unstimulated regions. The potassium flux in the extracellular space and glial compartment is negligible. b: Schematic graph of the water flux after the axon was stimulated. Note these graphs are graphs that summarize outputs of large numbers of calculations solving partial differential equations in longitudinal and radial spatial directions and time. They do not represent a compartmental model. They are the output of a model distributed in space.

In the Fig. 11f, in the extracellular space, potassium flows back to the stimulus region from the non-stimulus region via the extracellular pathway (in both cases). Accordingly, Fig. 12 shows that after the

Journal Pre-proof

axon stops firing, the water flow inside the compartments becomes almost zero. The water flows through both stimulated and unstimulated glial membrane into the glial compartment, which is the same as the schematic graph Fig. 13b.

In sum, after the axon stops firing action potentials, the extracellular potassium concentration is quickly transported in the glial compartment and extracellular pathway. The main clearance of potassium is through the glia membrane in both stimulated and unstimulated regions. The potassium flux through the extracellular pathway becomes weaker after the axon stops firing action potentials.

Fig. 14a&b, we show the variation of the potassium concentration in the extracellular stimulated and unstimulated regions, respectively. The peak potassium concentration in the stimulated region is higher in the outer stimulated case compared to the inner stimulated case. As discussed previously, the strength of potassium clearance is the same for both cases, while in the outer radial stimulated case, there is three times as much potassium in the extracellular space during the axon firing as in the inner radial stimulated case.

The equality of potassium clearance in both cases also explains why the potassium concentration drops faster in the inner radial stimulated case than the outer one after axon stop firing. We provide a decay timetable in the appendix.

Figure 14: a-b: potassium concentration variation in the extracellular stimulated region and non-stimulated region.

4.1.2. Randomly distributed stimulation

Spatially uniform patterns of stimulation might produce systematic artifacts as occur in Moire patterns and aliasing. In this section, we study whether random stimulation patterns in space differ from spatially uniform patterns. We apply a train of stimuli to four randomly distributed stimulated regions in the radial direction. The strength and duration of the stimulus is same as in the section 4.1.1 and the current is applied at the same longitudinal location $\left(z = z_0\right)$. The details of the radial stimulated location in each case is shown in Fig. 15.

Figure 15: The stimulated radial segments in each case. The intervals with value 1 are stimulated segments and the intervals with value 0 are unstimulated segments.

(a) During a train of axon firing

We compare the spatially random stimulated case (case 1, the rest of the cases are similar and shown in an appendix) with the inner radial region stimulated case in the Fig. 16a-d. During a train of axon firing, Fig. 16a&b, shows, in the randomly stimulated case, that the potassium clearance through the glial transmembrane $\left(M_S\right)$ has been reduced while the potassium flux through extracellular pathway in transition interface $\left(E_T\right)$ has dramatically increased. Fig. 16e&f shows that the major clearance pathway in the randomly stimulated cases becomes the extracellular pathway in transition interface $\left(E_T\right)$. More potassium flux goes though the extracellular path in the transition interface in comparison to how much goes through glial membrane in the stimulated region. This differs from the outer and inner stimulated cases, where the glial transmembrane $\left(M_S\right)$ dominates as seen in Fig. 6e&f.

Figure 16: a-d: the comparison between the spatially random stimulated case with the spatially uniform radial (inner) case during a train of axon firing. e-f: the cumulative flux comparison in M_S, E_T, M_{NS}, and G_T during a train of axon action potentials.

Fig. 16a-d shows that in the inner stimulated case (blue line), the potassium flux strength gradually increased with small oscillation in each axon stimulus time period, while in the spatially random stimulated case (red line), the potassium flux strength shows a periodic pattern in time with larger oscillation in each stimulus period. The reason for this quite different potassium flux pattern is that the extra potassium in the extracellular stimulated region has been cleared quicker in the random selected case. So, in each stimulus period, the potassium flux decreases dramatically since the potassium goes

Journal Pre-proof

back to its resting state. While in the inner stimulus case, for each stimulus period, the clearance of potassium is slower and there is accumulation of potassium in the stimulated extracellular space.

In sum, Fig. 16e&f, during a train of axon firing, much more potassium flux goes through the extracellular pathway through transition interface (E_T), which reduces the effect of glial compartment pathway in the stimulated region (M_S).

(b) After axon firing period

After the axon stops firing action potentials, both the spatially random case and the uniform inner case have similar reduced potassium fluxes, See M_S, E_T, M_{NS}, and G_T In Fig. 17e&g shows that the main pathway for potassium clearance (after the action potentials cease) is through the glial transmembrane pathway.

Figure 17: a-d: the comparison between the spatially random case with the uniform inner radial case after a train of action potentials Vector directions as defined previously. e-f: the cumulative flux comparison in M_S, E_T, M_{NS}, and G_T after a train of action potentials.

Fig. 17h shows a large difference between the spatially random and the spatially uniform case in some properties as we feared might occur. The cumulative transport of potassium flux through the glial compartment transition interface in the spatially random cases is much smaller than it is in the uniform inner case. This is because during axon firing period, the extracellular potassium in the stimulated region has been quickly removed in the random cases. The potassium concentration became more homogeneous and there was less difference between the stimulated region and non-stimulated regions. As a result, the glial compartment electric potential ϕ_{gl} becomes homogeneous in entire glial compartment and the electric drift flow in the glial transition interface was reduced for potassium. These results show the importance of checking for artifacts produced by artificial assumptions of spatial uniformity or periodicity.

(c) Potassium clearance and fluid velocity in the extracellular space and glial compartment

Since the potassium goes less through the glial transmembrane pathway in the stimulated region, the osmosis in the extracellular $k_B TO_{ex}$ and in glial $k_B TO_{gl}$, and variation in the stimulated region has been reduced. Therefore, the strength of the velocities decreases in both glia and extracellular compartment since the decrease of the glial transmembrane water flow as shown in Fig. 18c&d. The average potassium concentration changes in both stimulated region and non-stimulated region as shown in the Fig. 18a&b and its decay time in each case is in the appendix.

Figure 18: a-b: variation of potassium concentration in the extracellular simulated region and unstimulated regions. c-d: average glial compartment radial absolute velocity and extracellular space radial absolute velocity.

4.2. Effect of NKCC and non-selective pathway

In this section, we consider the effect of glial membrane conductance and a non-selective pathway on the pia boundary on the potassium clearance process. We first introduce the NKCC channel into the glial membrane, as widely studied in the literature. We compare simulation results between the model with NKCC and without NKCC. In the second part, we consider the effect of a non-selective pathway in the pia mater boundary. That pathway allows the convection flux through an extracellular pathway out of the optic nerve. We investigate how these factors affect the potassium clearance. While the contribution of the NKCC channel is significant, it is important to realize that in the present state of knowledge, other relevant channels may not yet have revealed themselves. Some channels become activated only under special conditions that are hard to find. Some channels may become activated only to protect systems under severe stress, as in clinical situations like oxygen deprivation, swelling, and so on. It will be important to identify such channels as the model is applied to clinical situations, some of which are of considerable importance.

4.2.1. Effect of NKCC on the glial membrane

We introduce a model of NKCC channels in the glial membrane as in the (29, 62), We describe the K^+, Na^+ and Cl^- flux through the NKCC channel in the glial membrane as in (29, 62)

$$J_{NKCC}^{K} = -\frac{I_{\max}^{NKCC}}{ez^{K}} \log\left(\frac{C_{ex}^{K}}{C_{gl}^{K}} \frac{C_{ex}^{Na}}{C_{gl}^{Na}} \left(\frac{C_{ex}^{Cl}}{C_{gl}^{Cl}}\right)^2\right),$$

$$J_{NKCC}^{Na} = -\frac{I_{\max}^{NKCC}}{ez^{Na}} \log\left(\frac{C_{ex}^{K}}{C_{gl}^{K}} \frac{C_{ex}^{Na}}{C_{gl}^{Na}} \left(\frac{C_{ex}^{Cl}}{C_{gl}^{Cl}}\right)^2\right), \qquad (28)$$

$$J_{NKCC}^{Cl} = 2\frac{I_{\max}^{NKCC}}{ez^{Cl}} \log\left(\frac{C_{ex}^{K}}{C_{gl}^{K}} \frac{C_{ex}^{Na}}{C_{gl}^{Na}} \left(\frac{C_{ex}^{Cl}}{C_{gl}^{Cl}}\right)^2\right).$$

To compare the effect of NKCC without NKCC, we keep the potassium and sodium concentration as well as the resting electric potential in the glial compartment and extracellular space the same. In the resting state, we set sodium and potassium current through NKCC channel to be comparable with respect to the Na/K pump current as in the paper (29, 62). In the appendix, we provide the two sets of parameters (NKCCa and NKCCb) that balance the additional NKCC current through the glial membrane.

In the simulation below, we compare the models with and without NKCC. The stimulated region Fig. 19, shows the cumulative potassium flux through the M_S, E_T, M_{NS}, and G_T during and after stimuli.

Figure 19: a-d: the cumulative flux comparison in M_S, E_T, M_{NS}, and G_T during a train of action potentials. e-h: the cumulative flux comparison in M_S, E_T, M_{NS}, and G_T after a train of action potentials.

Fig. 19a shows that more potassium goes through the glial membrane in the simulated region during axon firing when NKCC is present, which is hardly surprising. The NKCC channel has enhanced the transport of potassium through the glial membrane after the axon stopped firing as in Fig. 19e&g.

Fig. 4.13a&b shows the variation of potassium concentration in the extracellular space in the stimulated and unstimulated cases. The potassium decay in much faster when NKCC is present presumably because NKCC allows larger movement of potassium into the glial compartment. We provide the decay timetable in the appendix.

The quicker potassium is taken into glial compartment by the NKCC, the slower the return of potassium concentration back to resting state. Fig. 4.13c, shows the variation of the potassium concentration in the stimulated region. After action potentials cease, the potassium movement back to the axon compartment is reduced in the model with NKCC channel. Fig. 4.13c, shows that the average potassium concentration in the baseline model increases faster after the axon stops firing than in the model with NKCC.

Figure 20: a-b: extracellular potassium concentration variation comparison between the model with NKCC and baseline model (without NKCC). c: average potassium variation in the axon stimulated region.

4.2.2. Non-selective pathway through the pia matter

In this section, we consider the effect of a non-selective pathway across the pia boundary. The nonselective pathway allows both ion and water fluid transport through the cleft between the cells in the pia mater. We assume that the water fluid goes through the non-selective pathway only depends on the hydrostatic pressure difference. Therefore, the fluid condition on pia boundary (Γ_7) in (16) become

Journal Pre-proof

$$\boldsymbol{u}_{ex}^{OP}\cdot\hat{\boldsymbol{r}}=\boldsymbol{u}_{ex}^{SAS}\cdot\hat{\boldsymbol{r}}=u_{pia}^{m}+u_{pia}^{ns},\quad \text{on } \Gamma_7,$$

where

$$u_{pia}^{m}=L_{pia}^{m}\left(p_{ex}^{OP}-p_{ex}^{SAS}-\gamma_{pia}k_BT\left(O_{ex}^{OP}-O_{ex}^{SAS}\right)\right),$$

$$u_{pia}^{ns}=L_{pia}^{ns}\left(p_{ex}^{OP}-p_{ex}^{SAS}\right).$$

The non-selective pathway between the cell clefts provides an additional pathway for diffusion (∇C_l^i), electric drift ($C_l^i\nabla\phi_l$) as well as convection for ions ($C_l^i\boldsymbol{u}_l$). We modify the boundary condition (24) for ion on pia boundary $\left(\Gamma_7\right)$ as

$$\boldsymbol{j}_{ex}^{i,OP}\cdot\hat{\boldsymbol{r}}=\boldsymbol{j}_{ex}^{i,SAS}\cdot\hat{\boldsymbol{r}}$$

$$=\frac{G_{pia}^{i}+G^{ns}}{z^ie}\left(\phi_{ex}^{OP}-\phi_{ex}^{SAS}-E_{pia}^{i}\right)+c_{ex}^{i}u_{pia}^{ns},\ \text{on } \Gamma_7,$$

Here G^{ns} is the additional conductance due to the non-selective pathway and $C_{ex}^{i}u_{pia}^{ns}$ is the convection flux through the non-selective pathway on pia boundary.

In the simulation below, we compare the model with non-selective pathway with the model without the non-selective pathway. We choose the comparison parameter to be

$$\frac{G^{ns}}{G_{pia}^{K}}=\frac{L_{pia}^{ns}}{L_{pia}^{m}}=10.$$

In the Fig. 21, we show the potassium variation in extracellular space and the cumulative potassium flux through the pia mater and glial membrane.

Figure 21: a-b: extracellular potassium concentration variation comparison between the model with non-selective pathway on pia boundary and baseline model (without non-selective pathway).c: total cumulative potassium flux through glial membrane. d: total cumulative potassium flux though pia boundary.

The amount of potassium leak out of the optic nerve through the pia boundary is dramatically increased when the pathway is present in Fig. 21d. However, the dominant pathway of potassium clearance is still through the glial membrane as previously in Fig. 21c. This is because the total glial membrane area is much larger than the surface area on pia boundary,

$$\frac{2\pi R_aL}{V_{op}\mathcal{M}_{gl}}=O\left(10^{-3}\right),$$

where the V_on is the total optic nerve volume and M_gl is the glial membrane per unit volume. Fig. 21a&b shows that with the non-selective pathway on the pia boundary does not accelerate the potassium clearance rate very much.

5. Historical Comments and Discussion

There may be a concern about the large number of parameters in this and similar models. Models that contain large numbers of parameters can be difficult to compare and thus difficult to use in the scientific process of conjecture and refutation needed to understand these complex systems.

The need to deal with the complexity of the system as it is presented to us by evolution and used by animals should be clearly understood. Perhaps it is best understood by comparison with engineering systems. Engineering systems use enormous complexity—consider the 10^{13} components in our

computers and their connections—to perform specific functions. If the complexity is not described in a model, the model cannot describe the functions. Biological systems perform definite functions and use structures to do so. They are often devices in the exact engineering sense of the word. Complexity is needed to define these systems because without that complexity, the systems do not function.

Of course, the complexity cannot be uniquely defined in either engineering or biological systems. One can always appeal to an atomic description in the desperation of ignorance, but it is not at all clear that much detail helps, and the problems of dealing with irrelevant thermal motion, and difficulties in computation, have made such an approach so difficult that it is rarely used in engineering. Here we do the best we can by choosing structures and parameters that are needed considering their role in other similar biological systems.

The work here is done in the spirit of the structural analysis of physiological problems started by Falk and Fatt (63), continued by their student Eisenberg and his colleagues (64, 65) and applied to the lens of the eye with Rae and Mathias. This approach uses measured anatomical parameters (best by application of statistical sampling methods to biological systems, which was pioneered by Eisenberg and then extended generally by Brenda Eisenberg (66)), and impedance spectroscopy (67), to determine parameters exploiting the invariance of the capacitance (per unit area) of biological membranes. Mathias and his group showed how to extend these methods to include water flow (68, 69, 70) in a bidomain tissue, the lens of the eye. We extend that structural approach here to a tridomain model of an optic nerve.

In the electrical case, the parameters of a structural model are quite well specified by this approach. When dealing with water flow, it is important to include measurements of flow and pressure. In our situation the electrical information is available from the enormous knowledge of the properties of nerve fibers and action potential conduction developed since Hodgkin showed (71) that nerve conduction is electrical and not chemical (72). Measurements of pressure and flow are not available and they are surely needed if the model is to be further refined or extended to other analogous systems of the central nervous system, of great clinical importance. Measurements of a crucial property modified by water flow are possible thanks to the work of the Harvard group (Orkand et al). That work allows us to define our system as well as we have, but surely not well enough.

As this work is developed to become a model of the important phenomena of the recently discovered glymphatic system (20, 21), measurements of flow and pressure, as well as stereological measurements of structure and biophysical measurements of channel and pump distribution will assume crucial importance, in our view. Extensions of our theory and appropriate simplifications will also be helpful.

6. Conclusion

In this work, we propose a tridomain model to study potassium clearance in the optic nerve of Necturus in a series of experiments from Richard Orkand and the Harvard group (7, 8). Our model, analysis, and simulations provide a detailed picture of the role of glial cells in buffering the concentration of ions, mostly in the narrow extracellular space. While the nerve axons are being stimulated, both the extracellular space and glial cells play important roles. They both clear extra potassium from the narrow extracellular space while the axon is firing action potentials. After the action potentials stop, the potassium remaining in the extracellular space is cleared by the glial compartment.

Our model shows that the longitudinal electrical syncytium of the glial cells is critical for clearing potassium (from the extracellular space) when the neuron fires. The inward glial transmembrane potassium flux in the stimulated region is almost the same as the outward potassium flux out to the extracellular space in the non-stimulated region, in response to the change in potassium concentration between the extracellular space in the stimulated and unstimulated regions. This is because the electric potential spreads through the connected cells in the glial compartment. The glial electric potential in the unstimulated region becomes more positive in response to the depolarization of the glial electric potential in the stimulus region. The ‘syncytial properties’ of the glial compartment are a feature that separates our field model with its partial differential equations from the compartment models in the

literature that use ordinary differential equations. Compartment models lack the combination of space and time dependence needed to describe the temporal and spatial spread of potential. The combined temporal and spatial spread of potential is a crucial property of neurons. Here we show that the combined temporal and spatial spread of potential is a crucial property of the glia, and the narrow extracellular space between glia and neurons. In a sense, we extend the electrical cable theory used to describe the spatial spread of the electrical potential of neurons to a theory of spatial distribution of flow in neuron, glia, and the narrow extracellular space between them.

We discuss the effect of enhanced potassium conductance in the glial membrane and nerve membranes of the pia mater. On the one hand, incorporating NKCC channels into the glial membrane increases potassium clearance. Potassium clearance time is much shorter than that predicted by the baseline model (without NKCC channels in the glial membrane). On the other hand, an additional non-selective pathway in another location—in the pia mater—does not have significant effect on potassium clearance. This is not surprising since the total membrane area of the glial membrane in the optic nerve is much greater than the effective surface membrane of nerves in the pia mater.

Finally, our analysis of the model for the optic nerve is just a first small step towards the understanding of the mechanisms of the glial compartment buffering effect during the potassium clearance and microcirculation patterns of water and ions. The axons considered here is without myelin sheath. Myelin can be included by combining the model of myelinated nerve proposed in (58) as a first next step. Our distributed model and its partial differential equations can be generalized to describe ionic and water transport in tissues with more complicated and heterogeneous structures and with glymphatic pathways connected to the circulatory system. We expect that the spatially nonuniform distribution of ion and water channels and transporters will be used in many structures in the central nervous system to control flow. Obviously, at higher resolution much more detailed experimental observations and structure measurements (like pump distributions and membrane permeabilities) will be needed.

Author Contributions

Y.Z., S.X., and H.H. did the model derivations and carried out the numerical simulations. R.S.E. and H.H. designed the study, coordinated the study, and commented on the manuscript. All authors gave final approval for publication.

Acknowledgments

This research is supported in part by National Natural Science Foundation of China 12071190 and the Fundamental Research Funds for the Central Universities (S.X), the Fields Institute for Research in mathematical Science (S.X., R.S.E., and H.H.) and the Natural Sciences and Engineering Research Council of Canada (H.H.).

References

1. Hodgkin, A. L., A. F. Huxley, and B. Katz, 1952. Measurement of current-voltage relations in the membrane of the giant axon of Loligo. *The Journal of physiology* 116:424.

2. HODGKIN, A. i., 1949. Ionic currents underlying activity in the giant axon of the squid. *Arch. Sci. Physiol.* 3:129–150.

3. Hodgkin, A. L., and A. F. Huxley, 1952. Currents carried by sodium and potassium ions through the membrane of the giant axon of Loligo. *The Journal of physiology* 116:449–472.

4. Frankenhaeuser, B., and A. Hodgkin, 1956. The after-effects of impulses in the giant nerve fibres of Loligo. *The Journal of physiology* 131:341–376.

Journal Pre-proof

5. Hodgkin, A. L., and A. F. Huxley, 1952. A quantitative description of membrane current and its application to conduction and excitation in nerve. *The Journal of physiology* 117:500–544.

6. Kuffler, S. W., and J. G. Nicholls, 1966. The physiology of neuroglial cells. *In* Ergebnisse der physiologie biologischen chemie und experimentellen pharmakologie, Springer, 1–90.

7. Kuffler, S., J. Nicholls, and R. Orkand, 1966. Physiological properties of glial cells in the central nervous system of amphibia. *Journal of Neurophysiology* 29:768–787.

8. Orkand, R., J. Nicholls, and S. Kuffler, 1966. Effect of nerve impulses on the membrane potential of glial cells in the central nervous system of amphibia. *Journal of neurophysiology* 29:788–806.

9. Nedergaard, M., and S. A. Goldman, 2020. Glymphatic failure as a final common pathway to dementia. *Science* 370:50–56.

10. O'Connell, R., and Y. Mori, 2016. Effects of glia in a triphasic continuum model of cortical spreading depression. *Bulletin of mathematical biology* 78:1943–1967.

11. Tuttle, A., J. R. Diaz, and Y. Mori, 2019. A computational study on the role of glutamate and NMDA receptors on cortical spreading depression using a multidomain electrodiffusion model. *PLoS computational biology* 15:e1007455.

12. Ayata, C., and M. Lauritzen, 2015. Spreading depression, spreading depolarizations, and the cerebral vasculature. *Physiological reviews* 95:953–993.

13. Wei, Y., G. Ullah, and S. J. Schiff, 2014. Unification of neuronal spikes, seizures, and spreading depression. *Journal of Neuroscience* 34:11733–11743.

14. Ullah, G., Y. Wei, M. A. Dahlem, M. Wechselberger, and S. J. Schiff, 2015. The role of cell volume in the dynamics of seizure, spreading depression, and anoxic depolarization. *PLoS Comput Biol* 11:e1004414.

15. Mori, Y., 2015. A multidomain model for ionic electrodiffusion and osmosis with an application to cortical spreading depression. *Physica D: Nonlinear Phenomena* 308:94–108.

16. Miura, R. M., H. Huang, and J. J. Wylie, 2007. Cortical spreading depression: An enigma. *The European Physical Journal Special Topics* 147:287–302.

17. Gakuba, C., T. Gaberel, S. Goursaud, J. Bourges, C. Di Palma, A. Quenault, S. M. de Lizarrondo, D. Vivien, and M. Gauberti, 2018. General anesthesia inhibits the activity of the "glymphatic system". *Theranostics* 8:710.

18. Jiang, Q., L. Zhang, G. Ding, E. Davoodi-Bojd, Q. Li, L. Li, N. Sadry, M. Nedergaard, M. Chopp, and Z. Zhang, 2017. Impairment of the glymphatic system after diabetes. *Journal of Cerebral Blood Flow & Metabolism* 37:1326–1337.

Journal Pre-proof

19. Abbott, N. J., M. E. Pizzo, J. E. Preston, D. Janigro, and R. G. Thorne, 2018. The role of brain barriers in fluid movement in the CNS: is there a 'glymphatic'system? *Acta neuropathologica* 135:387–407.

20. Jessen, N. A., A. S. F. Munk, I. Lundgaard, and M. Nedergaard, 2015. The glymphatic system: a beginner's guide. *Neurochemical research* 40:2583–2599.

21. Mestre, H., Y. Mori, and M. Nedergaard, 2020. The brain's glymphatic system: current controversies. *Trends in Neurosciences* .

22. Tuckwell, H. C., and R. M. Miura, 1978. A mathematical model for spreading cortical depression. *Biophysical Journal* 23:257–276.

23. Postnov, D. E., L. S. Ryazanova, and O. V. Sosnovtseva, 2007. Functional modeling of neural–glial interaction. *BioSystems* 89:84–91.

24. Chang, J. C., K. C. Brennan, D. He, H. Huang, R. M. Miura, P. L. Wilson, and J. J. Wylie, 2013. A mathematical model of the metabolic and perfusion effects on cortical spreading depression. *PLoS One* 8:e70469.

25. Yao, W., H. Huang, and R. M. Miura, 2011. A continuum neuronal model for the instigation and propagation of cortical spreading depression. *Bulletin of mathematical biology* 73:2773–2790.

26. Bellinger, S., G. Miyazawa, and P. Steinmetz, 2008. Submyelin potassium accumulation may functionally block subsets of local axons during deep brain stimulation: a modeling study. *Journal of neural engineering* 5:263.

27. Chen, K. C., and C. Nicholson, 2000. Spatial buffering of potassium ions in brain extracellular space. *Biophysical journal* 78:2776–2797.

28. Reichenbach, A., J.-U. Stolzenburg, W. Eberhardt, T. Chao, D. Dettmer, and L. Hertz, 1993. What do retinal Müller (glial) cells do for their neuronal 'small siblings'? *Journal of chemical neuroanatomy* 6:201–213.

29. Østby, I., L. Øyehaug, G. T. Einevoll, E. A. Nagelhus, E. Plahte, T. Zeuthen, C. M. Lloyd, O. P. Ottersen, and S. W. Omholt, 2009. Astrocytic mechanisms explaining neural-activity-induced shrinkage of extraneuronal space. *PLoS computational biology* 5:e1000272.

30. Sibille, J., K. D. Duc, D. Holcman, and N. Rouach, 2015. The neuroglial potassium cycle during neurotransmission: role of Kir4. 1 channels. *PLoS computational biology* 11:e1004137.

31. Bellot-Saez, A., O. Kekesi, J. W. Morley, and Y. Buskila, 2017. Astrocytic modulation of neuronal excitability through K+ spatial buffering. *Neuroscience & Biobehavioral Reviews* 77:87–97.

32. Nicholson, C., and S. Hrabětová, 2017. Brain extracellular space: the final frontier of neuroscience. *Biophysical journal* 113:2133–2142.

Journal Pre-proof

33. Hou, R., Z. Zhang, D. Yang, H. Wang, W. Chen, Z. Li, J. Sang, S. Liu, Y. Cao, X. Xie, et al., 2016. Intracranial pressure (ICP) and optic nerve subarachnoid space pressure (ONSP) correlation in the optic nerve chamber: the Beijing Intracranial and Intraocular Pressure (iCOP) study. *brain research* 1635:201–208.

34. Morgan, W. H., C. Balaratnasingam, C. R. Lind, S. Colley, M. H. Kang, P. H. House, and D.-Y. Yu, 2016. Cerebrospinal fluid pressure and the eye. *British Journal of Ophthalmology* 100:71–77.

35. Killer, H., G. Jaggi, J. Flammer, N. R. Miller, A. Huber, and A. Mironov, 2006. Cerebrospinal fluid dynamics between the intracranial and the subarachnoid space of the optic nerve. Is it always bidirectional? *Brain* 130:514–520.

36. Band, L. R., C. L. Hall, G. Richardson, O. E. Jensen, J. H. Siggers, and A. J. Foss, 2009. Intracellular flow in optic nerve axons: a mechanism for cell death in glaucoma. *Investigative ophthalmology & visual science* 50:3750–3758.

37. Zhu, Y., S. Xu, R. S. Eisenberg, and H. Huang, 2019. A bidomain model for lens microcirculation. *Biophysical journal* 116:1171–1184.

38. Nicholson, C., 2001. Diffusion and related transport mechanisms in brain tissue. *Reports on progress in Physics* 64:815.

39. Filippidis, A. S., S. G. Zarogiannis, M. Ioannou, K. Gourgoulianis, P.-A. Molyvdas, and C. Hatzoglou, 2012. Permeability of the arachnoid and pia mater. The role of ion channels in the leptomeningeal physiology. *Child's Nervous System* 28:533–540.

40. Hayreh, S. S., 1984. The sheath of the optic nerve. *Ophthalmologica* 189:54–63.

41. Hayreh, S. S., 2009. Ischemic optic neuropathy. *Progress in retinal and eye research* 28:34–62.

42. Jonas, J. B., E. Berenshtein, and L. Holbach, 2003. Anatomic relationship between lamina cribrosa, intraocular space, and cerebrospinal fluid space. *Investigative ophthalmology & visual science* 44:5189–5195.

43. Xu, S., B. Eisenberg, Z. Song, and H. Huang, 2018. Osmosis through a semi-permeable membrane: a consistent approach to interactions. *arXiv preprint arXiv:1806.00646* .

44. Feher, J. J., 2017. Quantitative human physiology: an introduction. Academic press.

45. Hua, Y., A. P. Voorhees, and I. A. Sigal, 2018. Cerebrospinal fluid pressure: revisiting factors influencing optic nerve head biomechanics. *Investigative ophthalmology & visual science* 59:154–165.

46. Lu, Y.-B., K. Franze, G. Seifert, C. Steinhäuser, F. Kirchhoff, H. Wolburg, J. Guck, P. Janmey, E.-Q. Wei, J. Käs, et al., 2006. Viscoelastic properties of individual glial cells and neurons in the CNS. *Proceedings of the National Academy of Sciences* 103:17759–17764.

Journal Pre-proof

47. Feola, A. J., J. G. Myers, J. Raykin, L. Mulugeta, E. S. Nelson, B. C. Samuels, and C. R. Ethier, 2016. Finite element modeling of factors influencing optic nerve head deformation due to intracranial pressure. *Investigative ophthalmology & visual science* 57:1901–1911.

48. Eisenberg, B., Y. Hyon, and C. Liu, 2010. Energy variational analysis of ions in water and channels: Field theory for primitive models of complex ionic fluids. *The Journal of Chemical Physics* 133:104104.

49. Malcolm, D. T. K., 2006. A computational model of the ocular lens. Ph.D. thesis, ResearchSpace@ Auckland.

50. Mathias, R. T., 1985. Steady-state voltages, ion fluxes, and volume regulation in syncytial tissues. *Biophysical journal* 48:435.

51. Wan, L., S. Xu, M. Liao, C. Liu, and P. Sheng, 2014. Self-consistent approach to global charge neutrality in electrokinetics: A surface potential trap model. *Physical Review X* 4:011042.

52. Vaghefi, E., D. T. Malcolm, M. D. Jacobs, and P. J. Donaldson, 2012. Development of a 3D finite element model of lens microcirculation. *Biomedical engineering online* 11:69.

53. Pérez-Pinzón, M., L. Tao, and C. Nicholson, 1995. Extracellular potassium, volume fraction, and tortuosity in rat hippocampal CA1, CA3, and cortical slices during ischemia. *Journal of Neurophysiology* 74:565–573.

54. McLAUGHLIN, S., and R. T. Mathias, 1985. Electro-osmosis and the reabsorption of fluid in renal proximal tubules. *The Journal of general physiology* 85:699–728.

55. Gardiner, B. S., D. W. Smith, M. Coote, and J. G. Crowston, 2010. Computational modeling of fluid flow and intra-ocular pressure following glaucoma surgery. *PLoS One* 5:e13178.

56. Pache, M., and P. Meyer, 2006. Morphological changes of the retrobulbar optic nerve and its meningeal sheaths in glaucoma. *Ophthalmologica* 220:393–396.

57. Sigal, I. A., J. G. Flanagan, and C. R. Ethier, 2005. Factors influencing optic nerve head biomechanics. *Investigative ophthalmology & visual science* 46:4189–4199.

58. Song, Z., X. Cao, and H. Huang, 2018. Electroneutral models for dynamic Poisson-Nernst-Planck systems. *Physical Review E* 97:012411.

59. Fitzhugh, R., 1960. Thresholds and plateaus in the Hodgkin-Huxley nerve equations. *The Journal of general physiology* 43:867–896.

60. Gao, J., X. Sun, V. Yatsula, R. Wymore, and R. Mathias, 2000. Isoform-specific function and distribution of Na/K pumps in the frog lens epithelium. *The Journal of membrane biology* 178:89–101.

Journal Pre-proof

61. Kofuji, P., and E. A. Newman, 2004. Potassium buffering in the central nervous system. *Neuroscience* 129:1043–1054.

62. Lauf, P. K., and N. C. Adragna, 2000. K-Cl cotransport: properties and molecular mechanism. *Cellular Physiology and Biochemistry* 10:341–354.

63. Falk, G., and P. Fatt, 1964. Linear electrical properties of striated muscle fibres observed with intracellular electrodes. *Proceedings of the Royal Society of London. Series B. Biological Sciences* 160:69–123.

64. Schneider, M. F., 1970. Linear electrical properties of the transverse tubules and surface membrane of skeletal muscle fibers. *The Journal of general physiology* 56:640–671.

65. Valdiosera, R., C. Clausen, and R. Eisenberg, 1974. Impedance of frog skeletal muscle fibers in various solutions. *The Journal of general physiology* 63:460–491.

66. Eisenberg, B., and R. S. Eisenberg, 1968. Selective disruption of the sarcotubular system in frog sartorius muscle: a quantitative study with exogenous peroxidase as a marker. *The Journal of cell biology* 39:451–467.

67. Eisenberg, R., 2015. Electrical structure of biological cells and tissues: impedance spectroscopy, stereology, and singular perturbation theory. *arXiv preprint arXiv:1511.01339* .

68. Mathias, R., J. Rae, and R. Eisenberg, 1979. Electrical properties of structural components of the crystalline lens. *Biophysical Journal* 25:181–201.

69. Mathias, R., J. Rae, and R. Eisenberg, 1981. The lens as a nonuniform spherical syncytium. *Biophysical journal* 34:61–83.

70. Rae, J., R. Mathias, and R. Eisenberg, 1982. Physiological role of the membranes and extracellular space within the ocular lens. *Experimental eye research* 35:471–489.

71. Hodgkin, A., 1937. Evidence for electrical transmission in nerve: Part I. *The Journal of physiology* 90:183–210.

72. Hill, A. V., 1932. Chemical wave transmission in nerve. CUP Archive.

Supplementary Material

An online supplement to this article can be found by visiting BJ Online at `http://www.biophysj.org`.

Journal Pre-proof

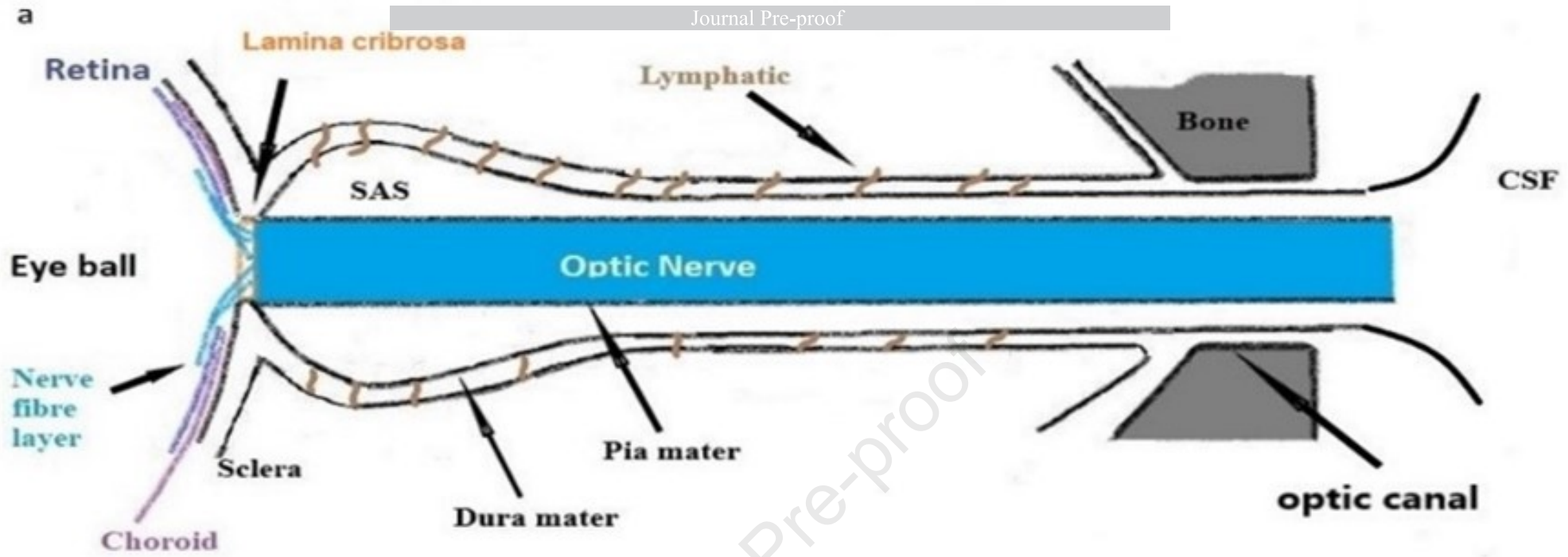

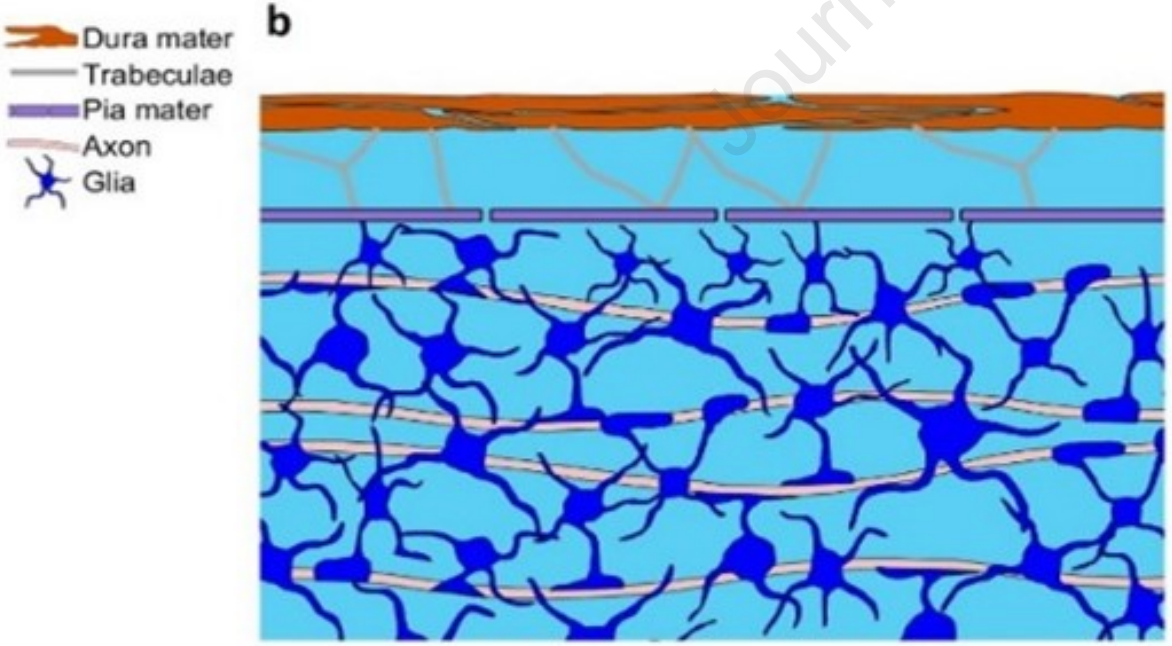

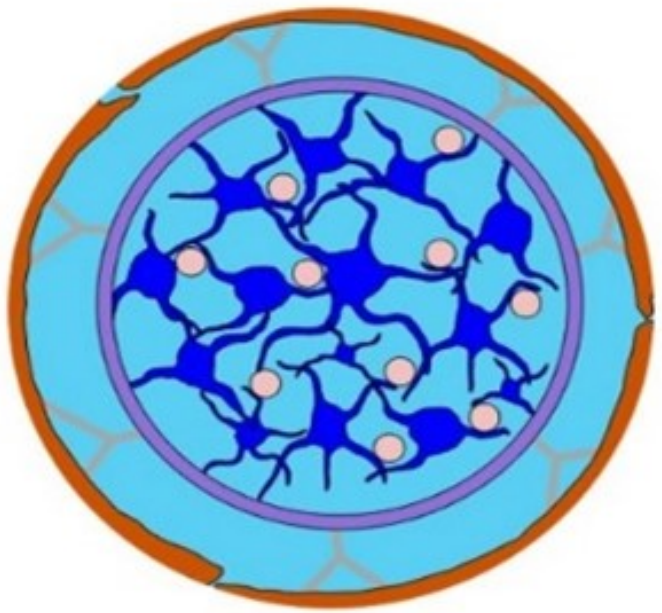

Journal Pre-proof
Journal Pre-proof

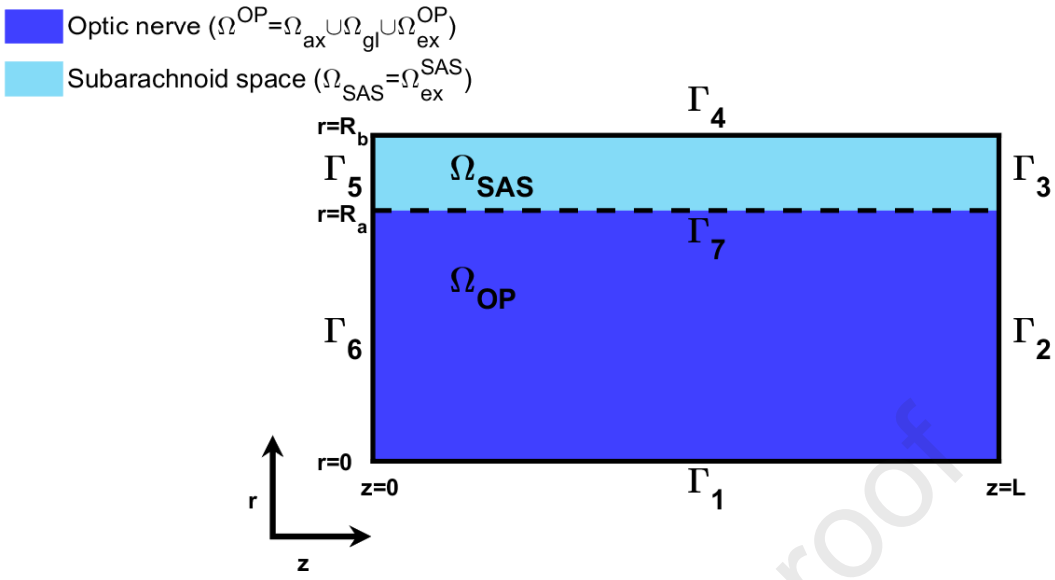

Journal Pre-proof

Journal Pre-proof

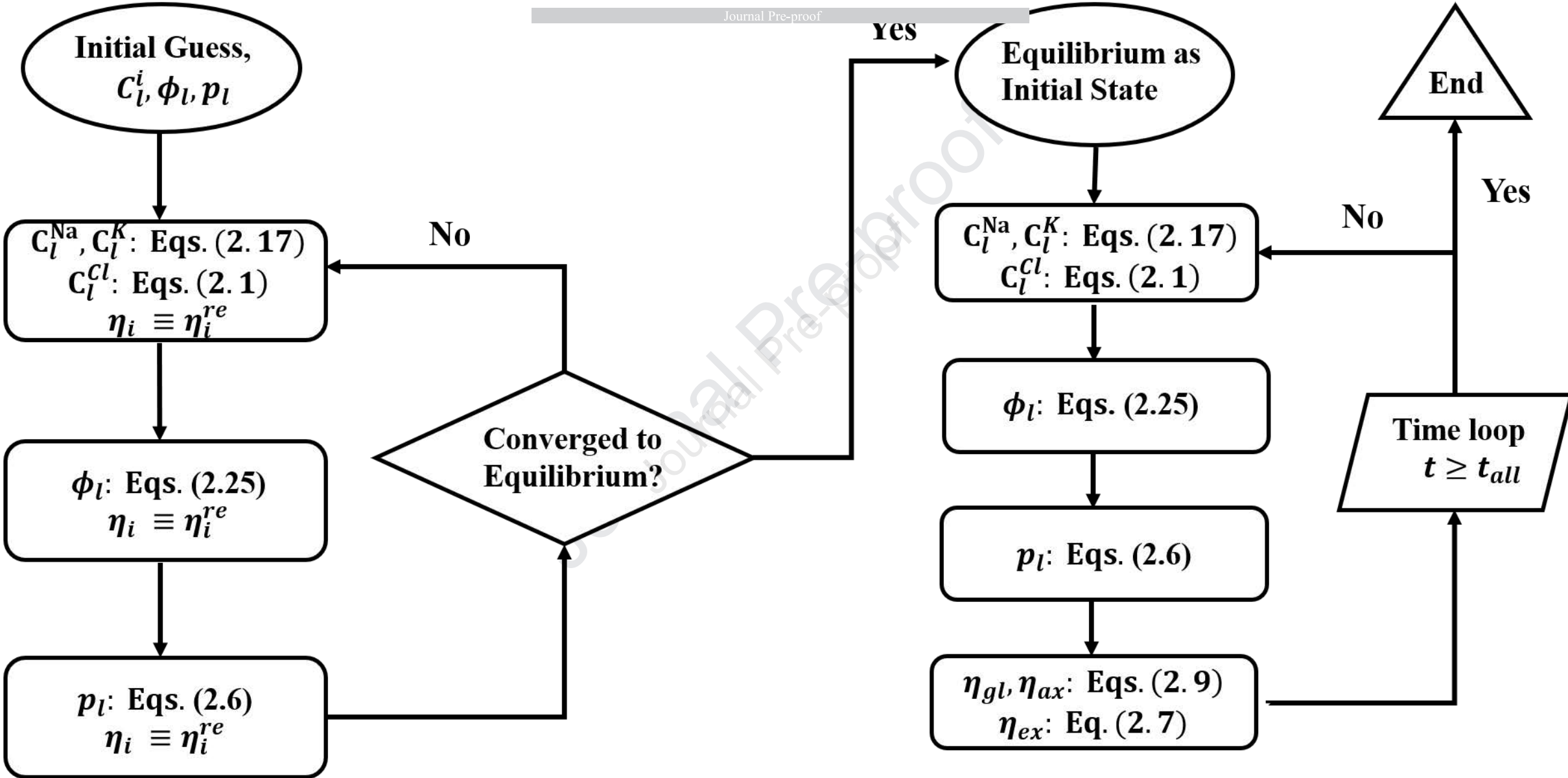

Journal Pre-proof
Journal Pre-proof

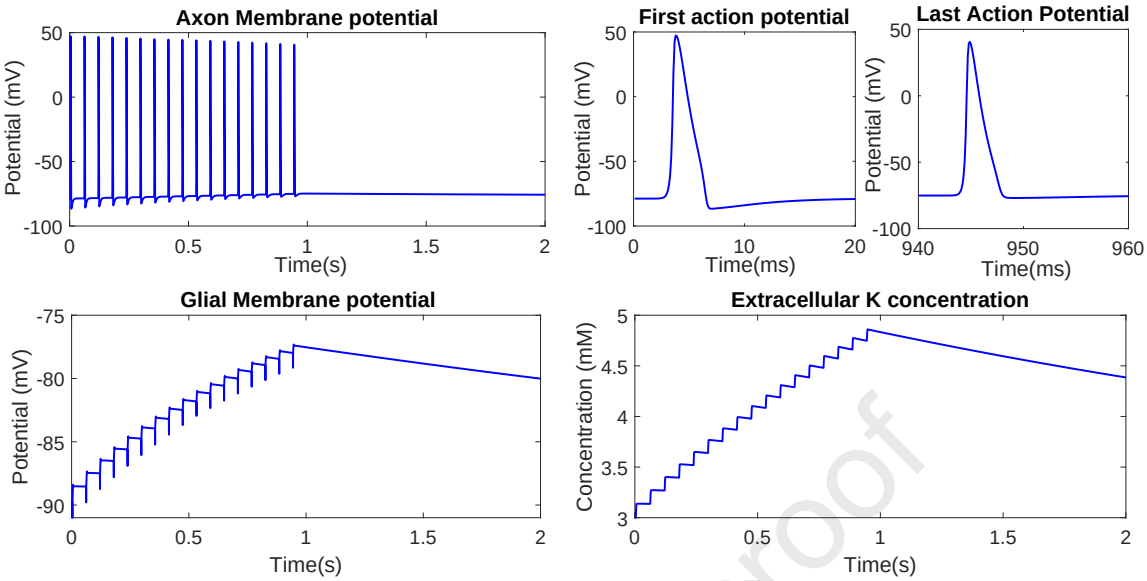

Journal Pre-proof

Journal Pre-proof
Journal Pre-proof

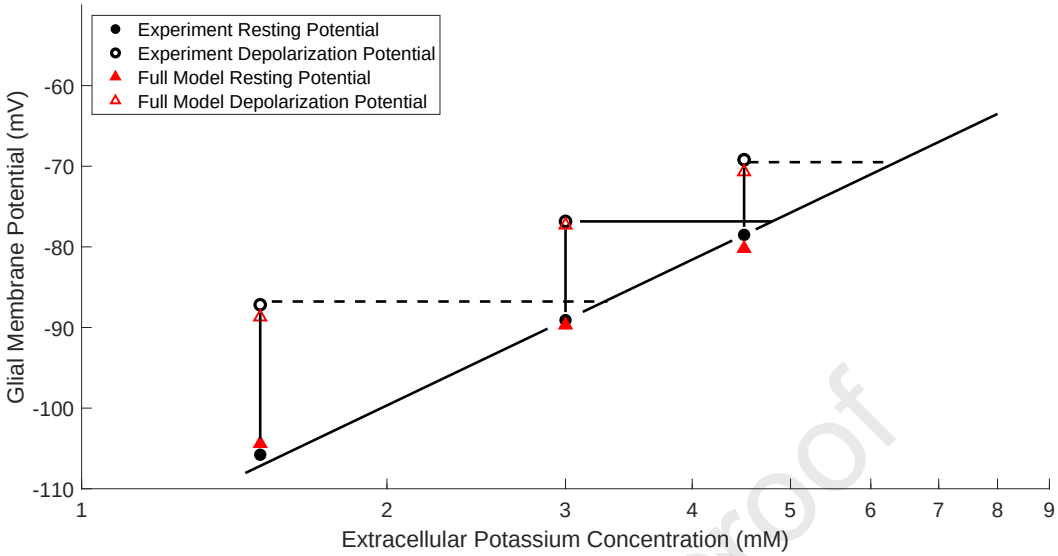

Journal Pre-proof

Journal Pre-proof
Journal Pre-proof

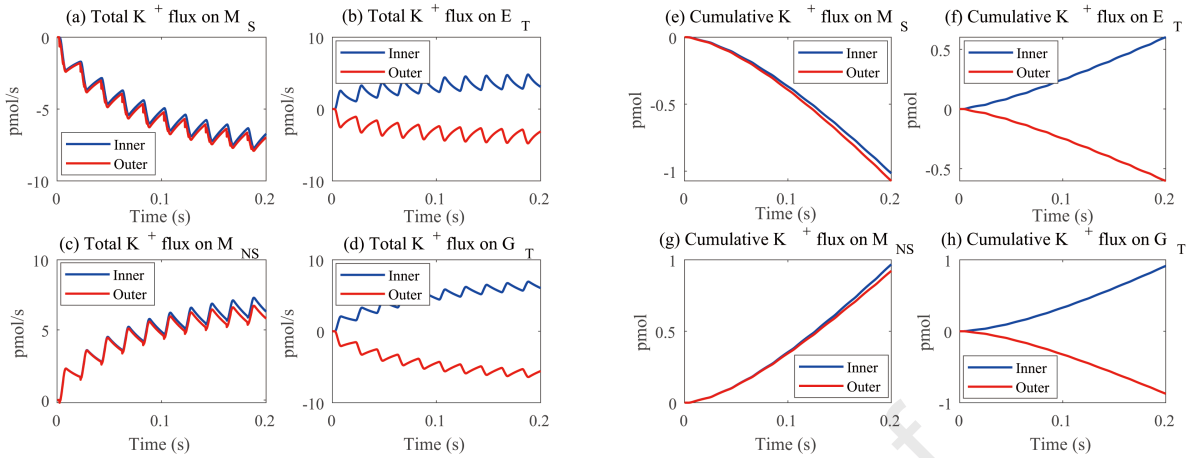

Journal Pre-proof

Journal Pre-proof
Journal Pre-proof

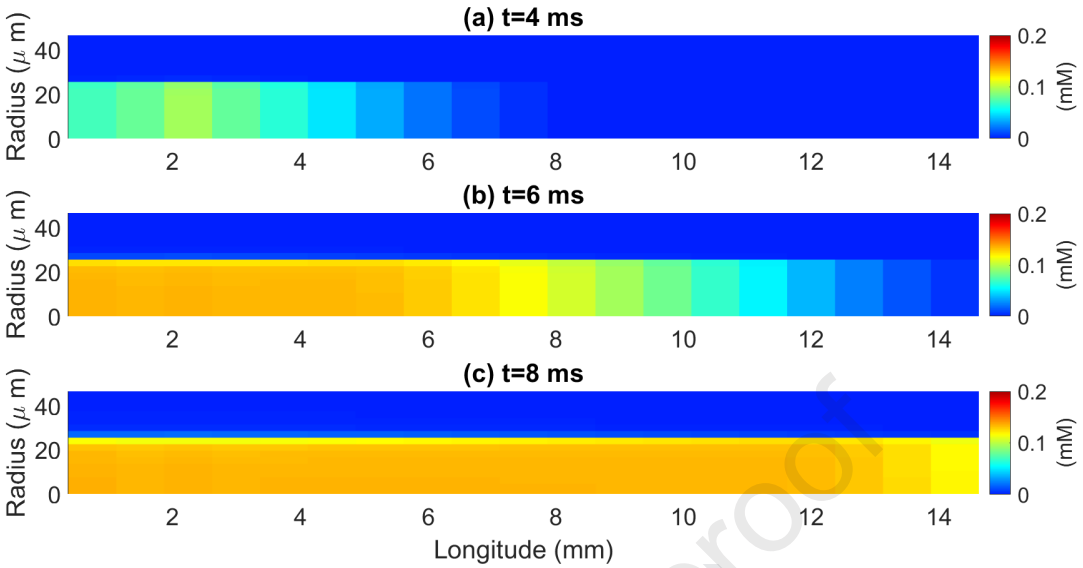

Journal Pre-proof

Journal Pre-proof
Journal Pre-proof

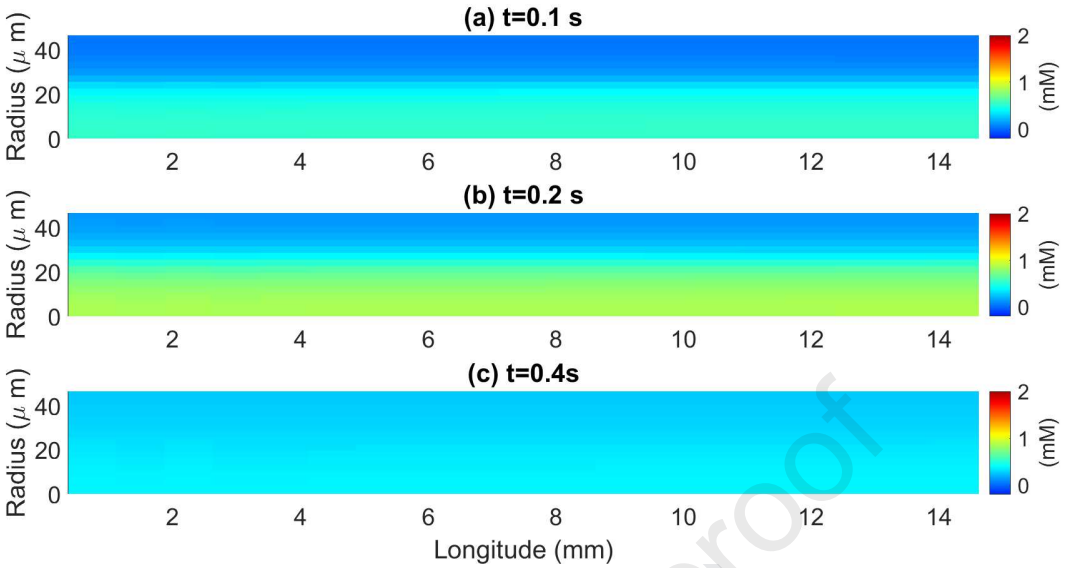

Journal Pre-proof

Journal Pre-proof
Journal Pre-proof

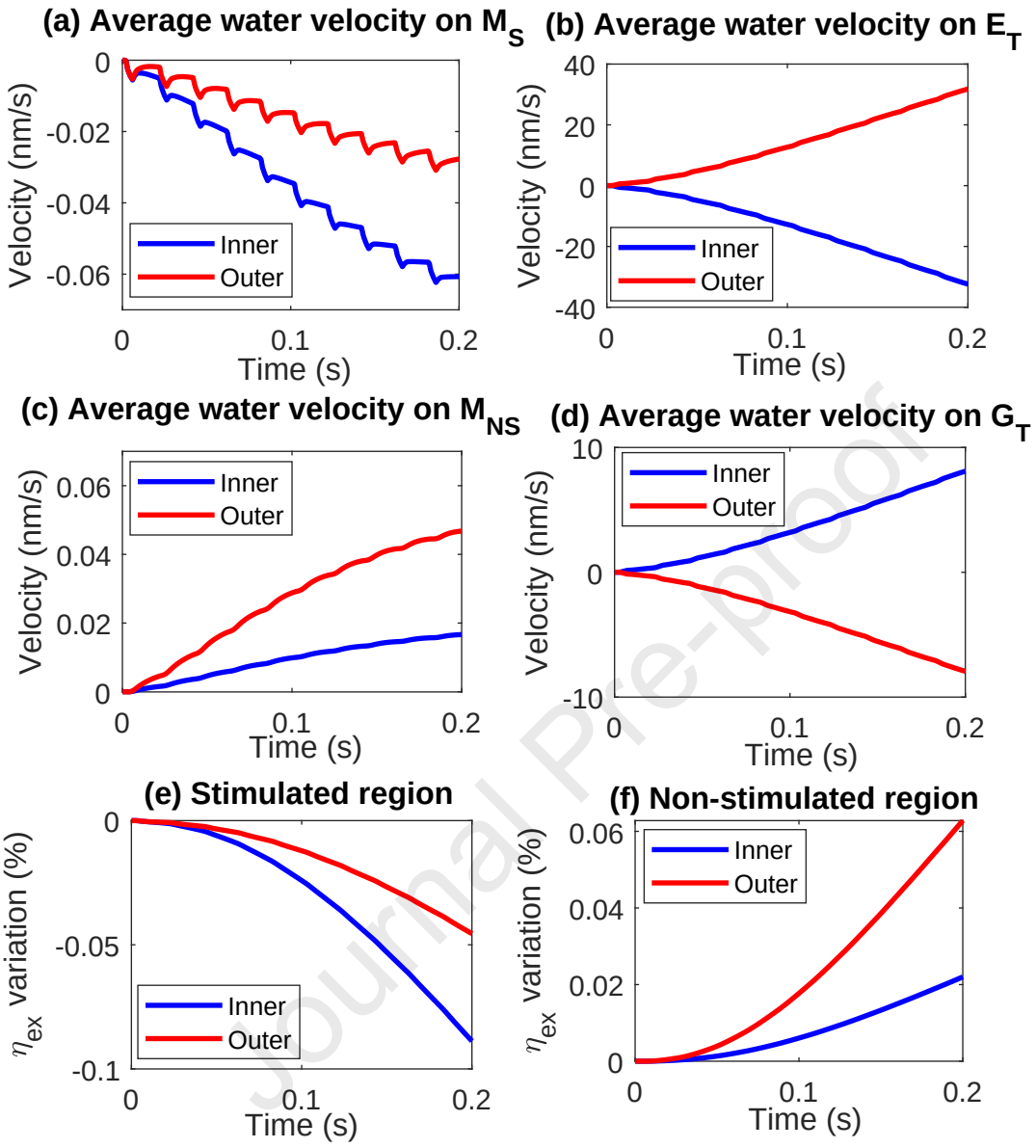

Journal Pre-proof

Journal Pre-proof

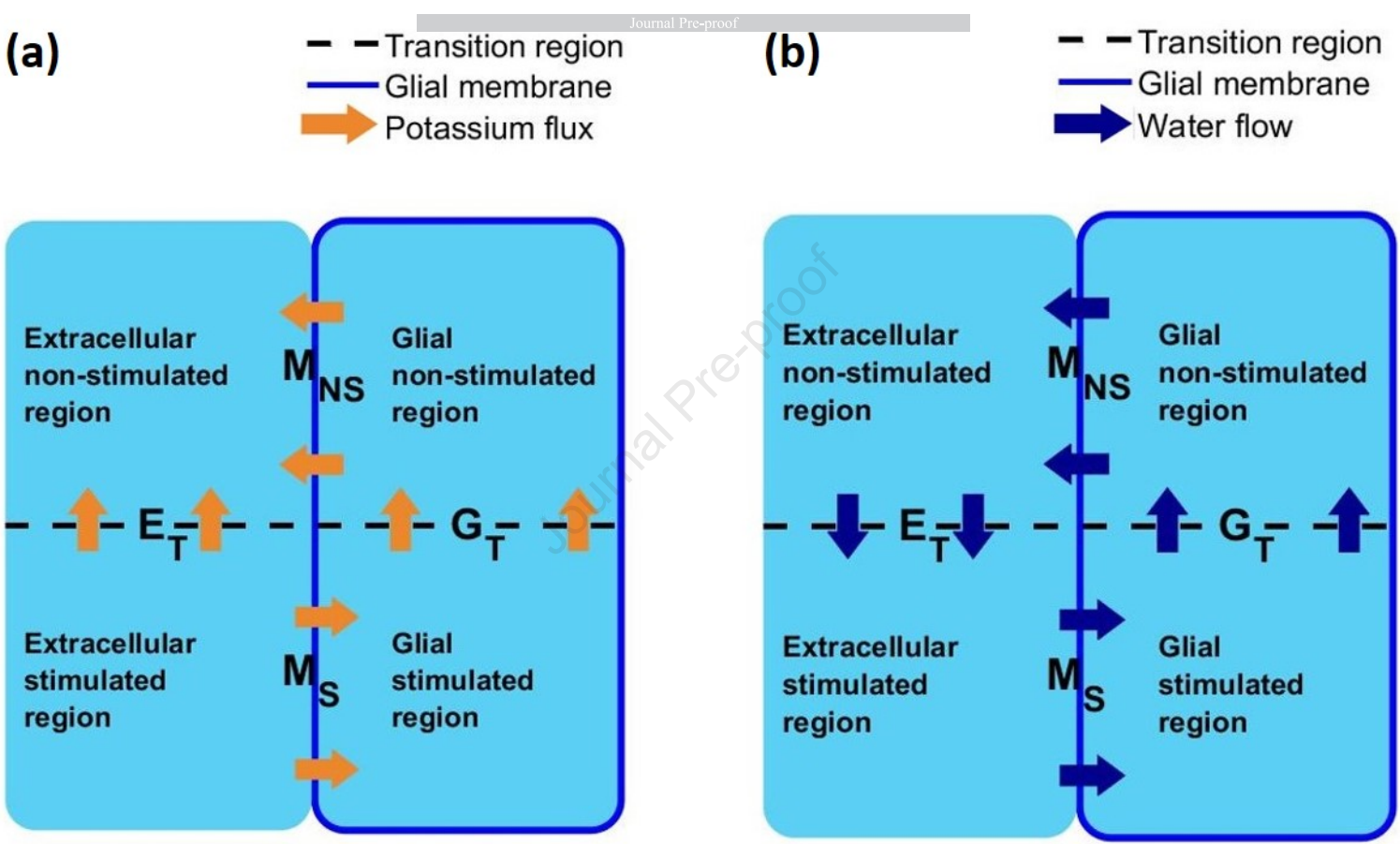

Journal Pre-proof

Journal Pre-proof
Journal Pre-proof

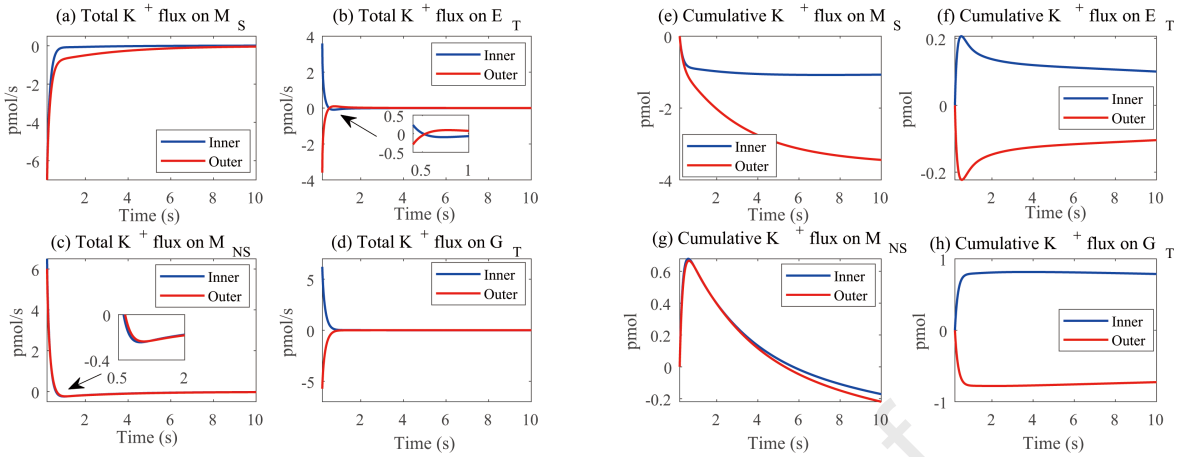

Journal Pre-proof

Journal Pre-proof

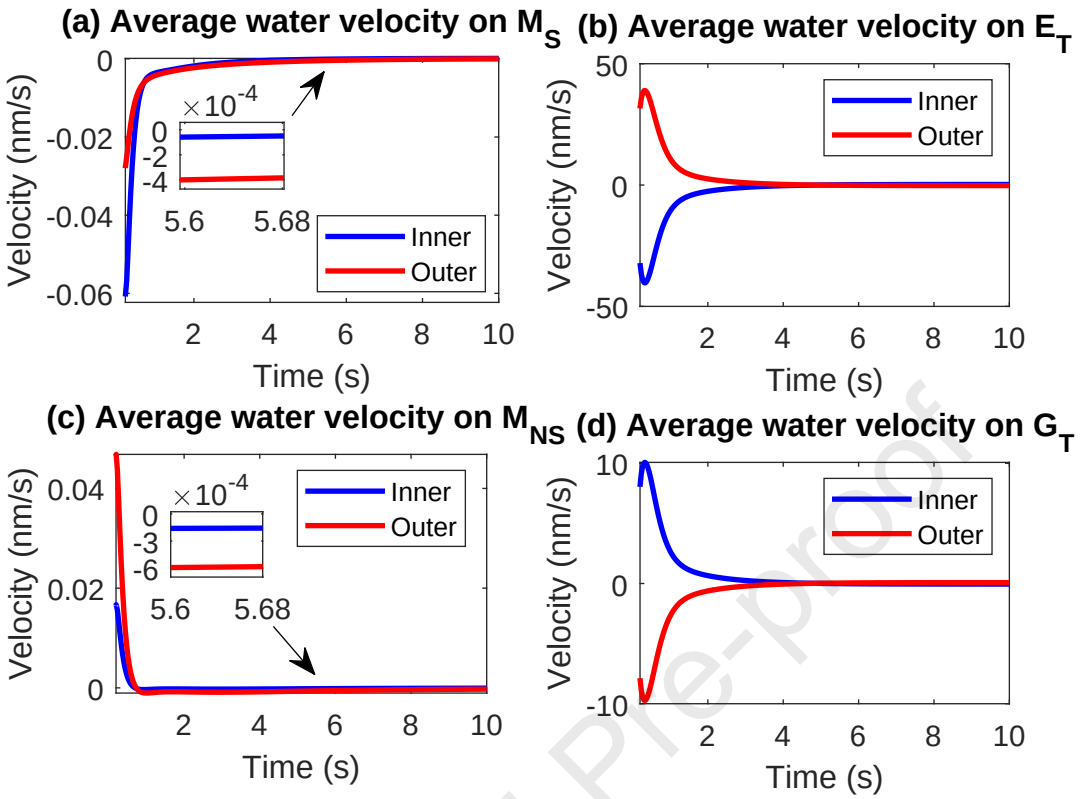

Journal Pre-proof

Journal Pre-proof

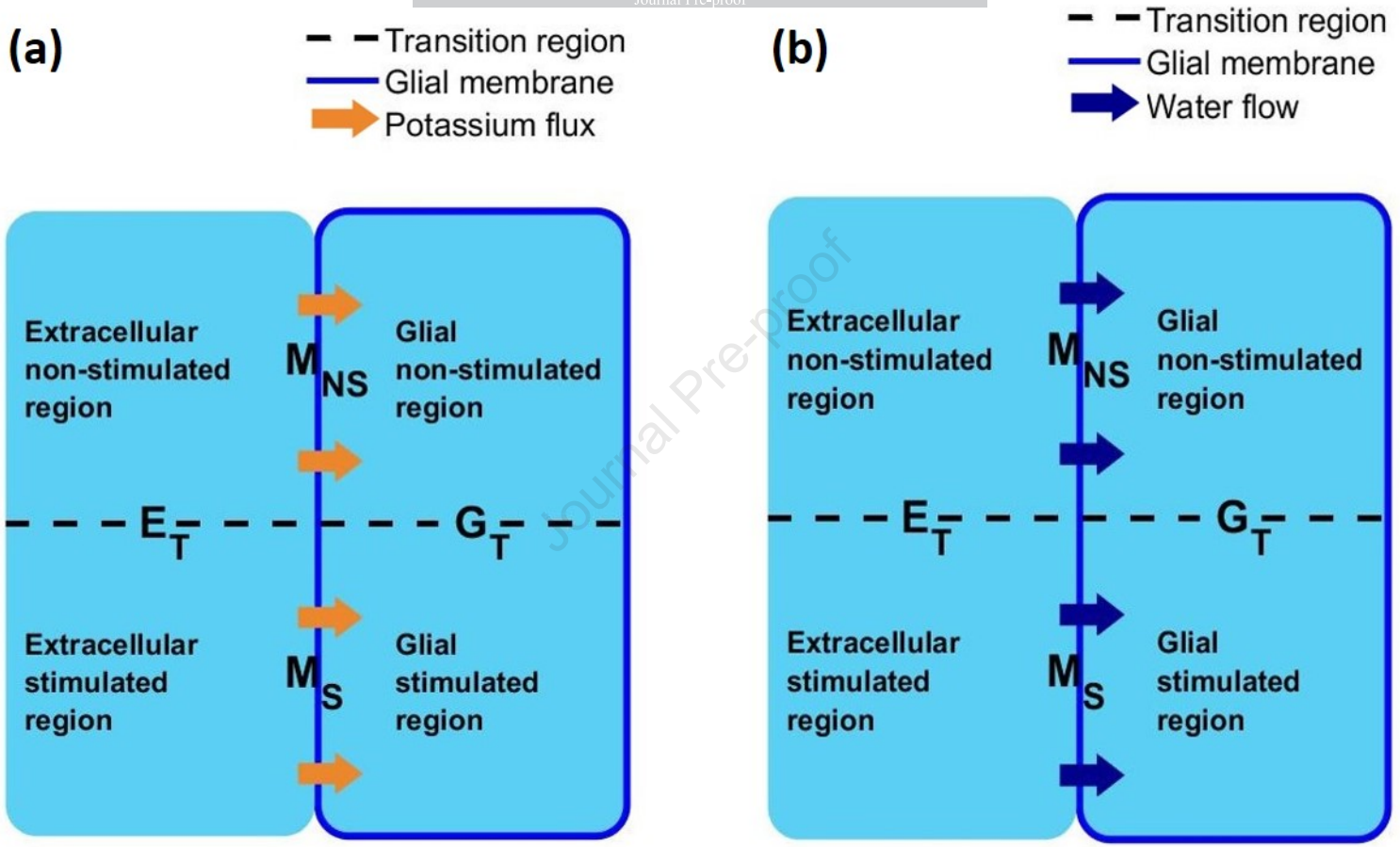

Journal Pre-proof

Journal Pre-proof
Journal Pre-proof

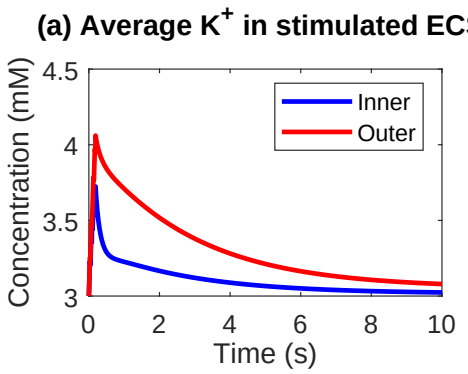

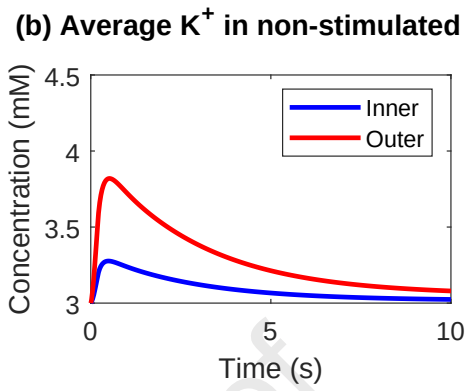

Journal Pre-proof

Journal Pre-proof
Journal Pre-proof

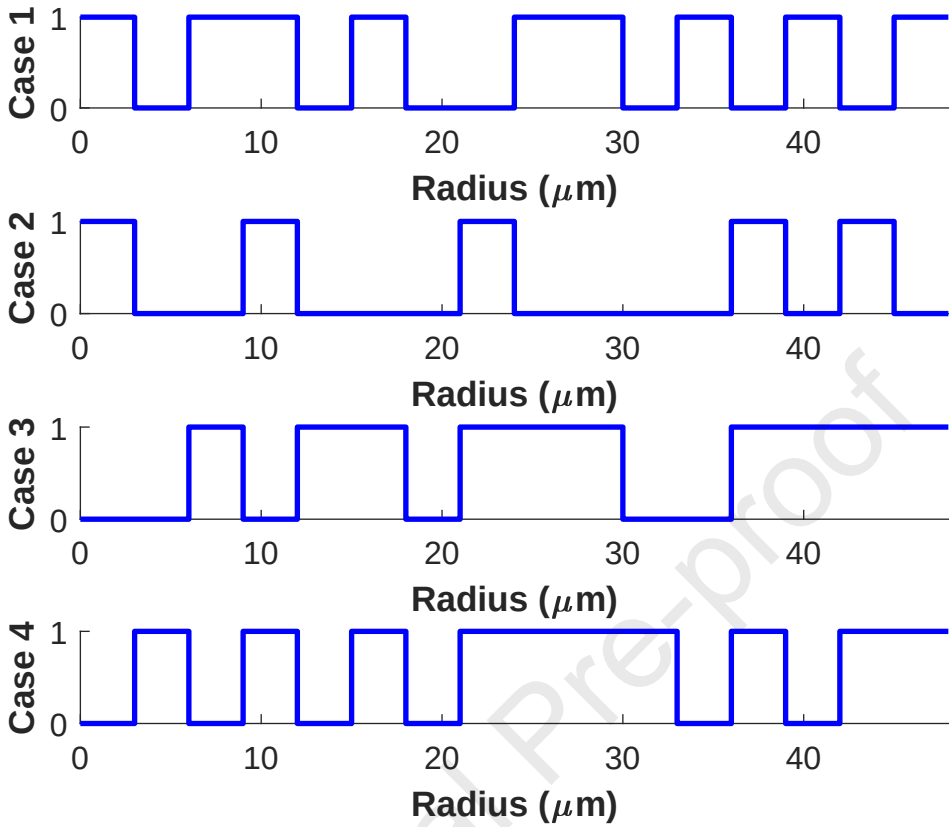

Journal Pre-proof

Journal Pre-proof
Journal Pre-proof

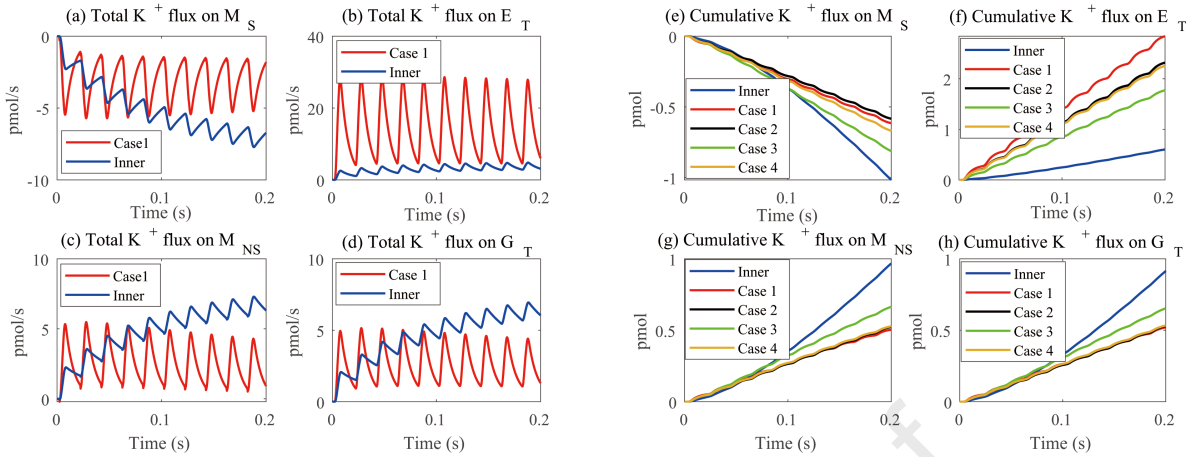

Journal Pre-proof

Journal Pre-proof
Journal Pre-proof

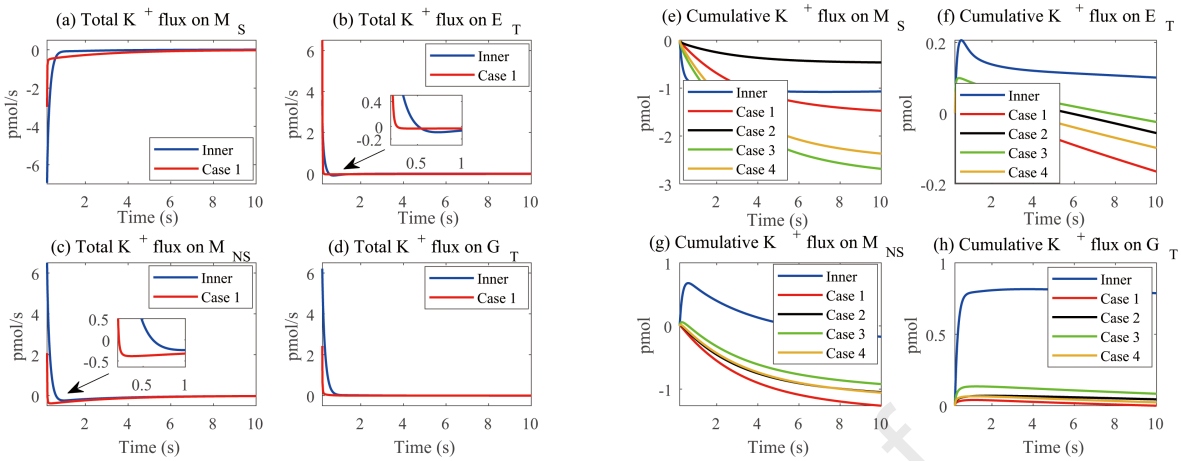

Journal Pre-proof

Journal Pre-proof
Journal Pre-proof

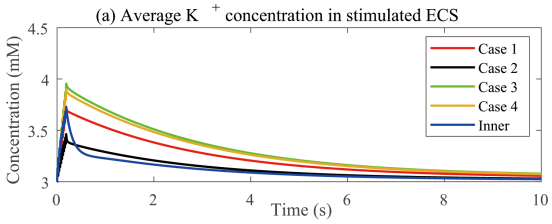

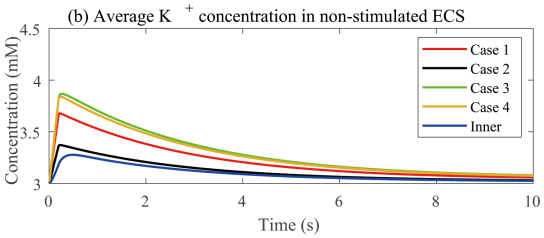

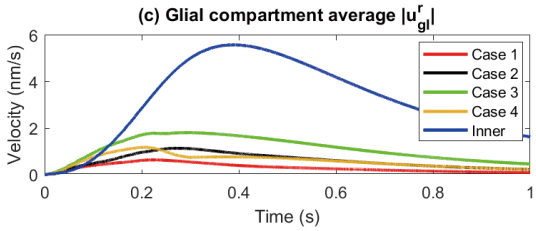

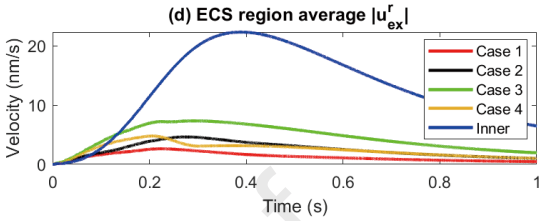

Journal Pre-proof

Journal Pre-proof
Journal Pre-proof

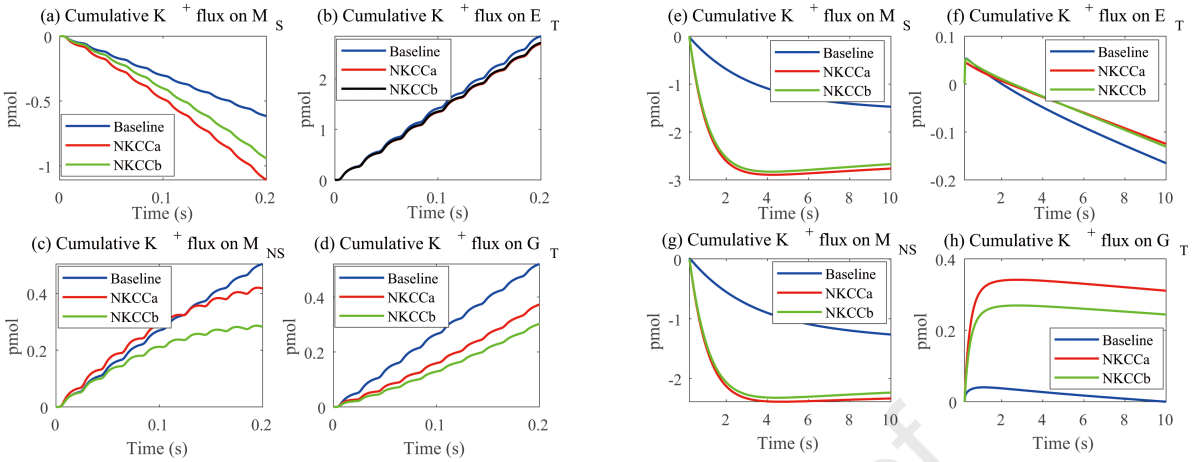

Journal Pre-proof

Journal Pre-proof
Journal Pre-proof

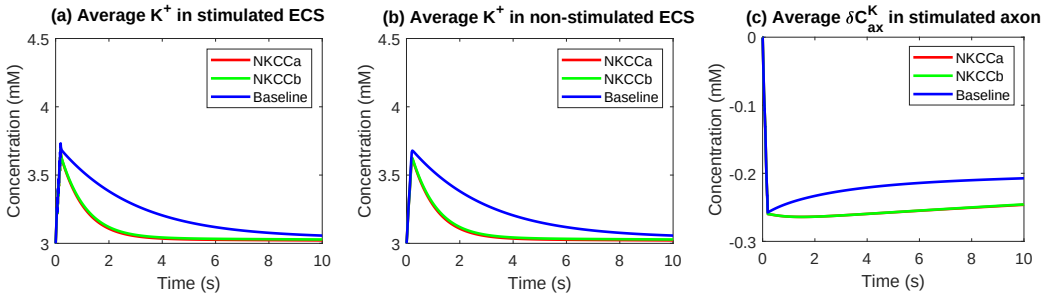

Journal Pre-proof

Journal Pre-proof
Journal Pre-proof

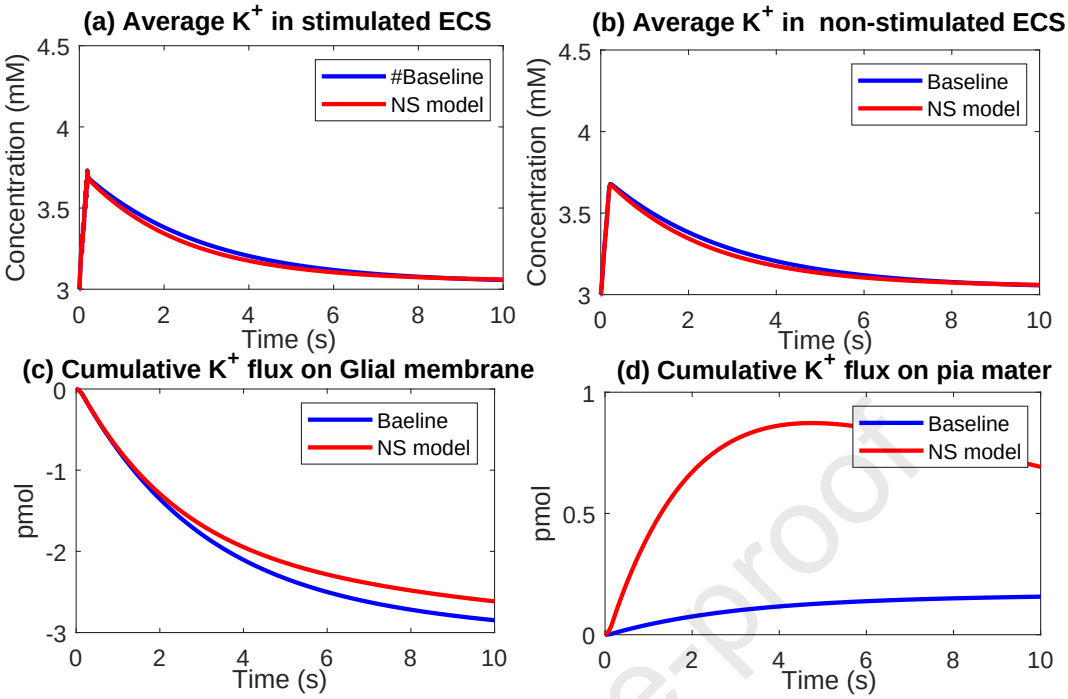

Journal Pre-proof